



Human model of IRX5 mutations reveals key role for this transcription factor in ventricular conduction

Zeina R Al Sayed, Robin Canac, Bastien Cimarosti, Carine Bonnard, Jean-Baptiste Gourraud, Hanan Hamamy, Hulya Kayserili, Aurore Girardeau, Mariam Jouni, Nicolas Jacob, et al.

► To cite this version:

Zeina R Al Sayed, Robin Canac, Bastien Cimarosti, Carine Bonnard, Jean-Baptiste Gourraud, et al.. Human model of IRX5 mutations reveals key role for this transcription factor in ventricular conduction. Cardiovascular Research, 2021, 117 (9), pp.2092-2107. 10.1093/cvr/cvaa259 . inserm-02934863v2

HAL Id: inserm-02934863

<https://inserm.hal.science/inserm-02934863v2>

Submitted on 8 Nov 2021

HAL is a multi-disciplinary open access archive for the deposit and dissemination of scientific research documents, whether they are published or not. The documents may come from teaching and research institutions in France or abroad, or from public or private research centers.

L'archive ouverte pluridisciplinaire **HAL**, est destinée au dépôt et à la diffusion de documents scientifiques de niveau recherche, publiés ou non, émanant des établissements d'enseignement et de recherche français ou étrangers, des laboratoires publics ou privés.

Human model of *IRX5* mutations reveals key role for this transcription factor in ventricular conduction

Zeina R Al Sayed, PhD¹, Robin Canac, MSc¹, Bastien Cimarosti, MSc¹, Carine Bonnard, PhD², Hanan Hamamy, MD³, Hulya Kayserili, MD-PhD⁴, Aurore Girardeau, BSc¹, Mariam Jouni¹, PhD, Nicolas Jacob, MD¹, Anne Gaignerie, MSc⁵, Caroline Chariou, BSc⁵, Laurent David, PhD⁵⁻⁷, Virginie Forest, PhD¹, Céline Marionneau, PhD¹, Gildas Loussouarn, PhD¹, Guillaume Lamirault, MD-PhD¹, Bruno Reversade, PhD^{2,4,8-10}, Kazem Zibara, PhD¹¹, Patricia Lemarchand, MD-PhD^{1,12*}, Nathalie Gaborit, PhD^{1*}

1. l'institut du thorax, INSERM, CNRS, UNIV Nantes, Nantes, France.
2. Institute of Medical Biology, A*STAR, Singapore, Singapore.
3. Department of Genetic Medicine and Development, Geneva University, Geneva 1211, Switzerland.
4. Medical Genetics Department, Koç University School of Medicine (KUSOM), Istanbul, Turkey.
5. SFR-Santé François Bonamy, INSERM, CNRS, UNIV Nantes, CHU Nantes, Nantes, France.
6. CRTI, INSERM, UNIV Nantes, Nantes, France.
7. ITUN, CHU Nantes, Nantes, France.
8. Department of Paediatrics, National, University of Singapore, Singapore, Singapore.
9. Institute of Molecular and Cellular Biology, A*STAR, Singapore, Singapore.
10. Reproductive Biology Laboratory, Amsterdam UMC, Amsterdam-Zuidoost, Netherlands.
11. ER045, Laboratory of stem cells, DSST, Biology department, Faculty of Sciences, Lebanese University, Beirut, Lebanon.
12. l'institut du thorax, CHU Nantes, Nantes, France.

Short title: Key role of *IRX5* in human ventricular conduction

Total word count: 8992

Manuscript category: Original article

Reprint requests and correspondence:

Nathalie GABORIT, PhD and Patricia Lemarchand, MD-PhD

l'institut du thorax

Inserm UMR 1087, CNRS UMR 6291

IRS-UN, 8 quai Moncousu

44007 Nantes cedex 1, France

E-mail: nathalie.gaborit@univ-nantes.fr and patricia.lemarchand@univ-nantes.fr

Abstract

Aim: Several inherited arrhythmic diseases have been linked to single gene mutations in cardiac ion channels and interacting proteins. However, the mechanisms underlying most arrhythmias, are thought to involve altered expression regulation of multiple effectors. In this study, we aimed to examine the role of a transcription factor belonging to the Iroquois homeobox family, IRX5, in cardiac electrical function.

Methods and results: Using human cardiac tissues, transcriptomic correlative analyses between IRX5 and genes involved in cardiac electrical activity showed that in human ventricular compartment, *IRX5* expression strongly correlated to the expression of major actors of cardiac conduction, including the sodium channel, Nav1.5, and Connexin 40 (Cx40). We then generated human induced pluripotent stem cells (hiPSCs) derived from two Hamamy Syndrome-affected patients carrying distinct homozygous loss-of-function mutations in *IRX5* gene. Cardiomyocytes derived from these hiPSCs showed impaired cardiac gene expression program, including dysregulation in the control of Nav1.5, Cx40 and Cx43 expression. In accordance with the prolonged QRS interval observed in Hamamy Syndrome patients, a slower ventricular action potential depolarization due to sodium current reduction was observed on electrophysiological analyses performed on patient-derived cardiomyocytes, confirming the functional role of IRX5 in electrical conduction. Finally, a novel cardiac transcription factor complex was identified, composed by IRX5 and GATA4, in which IRX5 potentiated GATA4-induced expression of *SCN5A*.

Conclusions: Altogether, this work unveils a key role for IRX5 in the regulation of human ventricular depolarization and cardiac electrical conduction, providing therefore new insights into our understanding of cardiac diseases.

Keywords:

IRX5, transcription factors, conduction, arrhythmia, Hamamy syndrome, human induced pluripotent stem cells.

27 **Translational perspectives**

28 Inherited cardiac arrhythmias account for about 20% of sudden cardiac deaths, of which a small
29 portion are monogenic familial diseases with mutations in cardiac ion channels. However,
30 pathogeny of inherited cardiac arrhythmias is increasingly thought to result from complex
31 mechanisms involving altered expression regulation of multiple effectors. Taking advantage of
32 cardiomyocytes derived from Hamamy syndrome patients, carrying loss-of-function mutations
33 in *IRX5* transcription factor, we uncovered an important role for IRX5 in the regulation of
34 several major players of ventricular depolarization conduction and in arrhythmogenesis. Thus,
35 this study supports systematic screening for genetic variants in IRX5 in inherited cardiac
36 arrhythmias.

1. Introduction

Inherited cardiac arrhythmias account for about 20% of sudden cardiac deaths. Only a small portion of these arrhythmias are monogenic familial diseases, having been successfully linked to rare mutations in cardiac ion channels and related proteins [1]. However, pathogeny of inherited cardiac arrhythmias is increasingly thought to be based on complex mechanisms involving polygenic inheritance and/or altered expression regulation of multiple effectors [2]. In this context, investigating how dysfunction of transcriptional regulators participates in the mechanism of these diseases is of major importance.

The regulation of global cardiac electrical transcriptional program, including ion channels and gap junctions, is a major determinant of proper initiation and propagation of action potential (AP) through the cardiac muscle. In animal models, several transcription factors (TFs) have been shown to play mechanistic roles in cardiac electrical activity and arrhythmias [3,4], including members of the Iroquois (IRX) family of TFs [5].

Autosomal recessive mutations in *IRX5*, an Iroquois homeobox TF, cause an inherited congenital disorder named Hamamy Syndrome (HMMS, OMIM611174) which clinical description revealed on the electrocardiogram, a QRS prolongation, illustrating a delayed ventricular electrical conduction, and a bradycardia [6,7]. Surprisingly, in mice, deletion of *Irx5* leads to a different phenotype, a ventricular repolarization defect, due to the role of *Irx5* in controlling potassium channel gene expression [8]. Inversely, another murine member of the *Irx* family, *Irx3*, is essential for fine regulation of intercellular coupling within the ventricular conduction system, through the regulation of connexins expression [9,10]. This suggests that distinct regulatory pathways govern the differences between human and animal cardiac electrical physiology.

In this study, our goal was to decipher whether IRX5 controls human cardiac electrical activity. First, correlative transcriptomic analyses between IRX5 and cardiac electrophysiology genes in human cardiac tissues, suggested that IRX5 may regulate several major actors of cardiac conduction. Then, human induced pluripotent stem cells (hiPSCs) derived from HMMS patients carrying *IRX5* mutations were used to elucidate the role of IRX5 in regulating expression of these actors of cardiac conduction and to uncover a cooperative activity between TFs. This work reveals how LOF mutation in one key TF affects the expression of multiple effectors of ventricular electrical conduction and improves our understanding of cardiac disease, paving the way therefore for more effective therapies.

2. Methods

Ethical Statement:

The study was conducted according to the principles set forth under the Declaration of Helsinki (1989) and European guidelines for clinical and genetic research. Institutional review board approvals of the study were obtained before the initiation of patient enrollment. Regarding the patient-derived biological samples, signed informed consent allowing the experiments to be conducted have been received from all individuals. Any related health information was collected in compliance with applicable law/regulation and with any applicable policy of the ethics committee with jurisdiction over the biological sample collection. All biological samples and their related health information have been provided in coded form such that subjects cannot be identified directly. The provisions of French law, article L1110-4 of the Code de la santé publique, related to the privacy and confidentiality of information regarding patients, have been observed. The transfer of the Hamamy syndrome-affected (HMMS) patient's biological samples has complied with all applicable laws as well as legal, regulatory and ethical requirements in transferring and obtaining such Material and the corresponding informed consents (Authorization IE 2009-505(1)).

2.1 Transcriptional analysis of human and murine tissues

RNA sequencing data in human heart were collected from the GTEx portal website (<http://gtexportal.org>). Briefly, transcripts per million (TPM) were downloaded for 297 atrial and 303 ventricular available tissue samples.

Regarding murine samples, animal experiments were performed in accordance with institutional guidelines for animal use in research. Hearts were excised from six 10-week-old C57BL/6 male mice and atria and ventricles were carefully dissected as previously described [11].

Two-way hierarchical agglomerative clustering was applied to gene-expression matrices (see TLDA section below), by centering gene expression values on the values-median and using average linkage-clustering with uncentered correlation (Cluster 3.0). GTEx left ventricular tissues RNA sequencing data of major cardiac sodium channels and connexins were ranked according to ascending expression of IRX5. Expression correlations were tested using Pearson correlation package on R software.

2.2 Human induced pluripotent stem cells (hiPSC) generation

Primary dermal fibroblasts were derived from skin biopsies were obtained from donors of two different consanguineous families, previously described with Hamamy Syndrome [6,7]. The first diseased donor is a 4-year-old boy, homozygous carrier of the c.448G>C *IRX5* mutation (p.Ala150Pro annotated as A150P) in whom a QRS prolongation on the ECG was diagnosed. The second donor is a 17-year-old boy belonging to another family harboring the homozygous c.498C>A *IRX5* mutation (p.Asn166Lys annotated as N166K) who presents a prolonged QRS duration on the ECG, in addition to a tiny patent ductus arteriosus. In parallel, fibroblasts from three individuals lacking the *IRX5* mutations were used as controls: the unaffected sister of the first donor, a healthy subject with comparable gender, age, and ethnicity as second donor, as well as an unrelated previously described control [13]. HiPSC lines were generated using Sendai virus method. For each line, two to three hiPSC clones were selected and expanded on stem cell-qualified Matrigel-coated plates (0.1 mg/ml; BD Bioscience) with StemMACS™ iPS Brew XF medium (Miltenyi Biotec).

2.3 HiPSC characterization

For all clones, genomic DNA was extracted and mutations were verified by sequencing using primers specific for the genomic regions surrounding the A150P and N166K mutations (Supplemental Table 1). Pluripotency marker gene expression was assessed using flow cytometry, qRT-PCR, and immunofluorescence as previously described [13]. Single nucleotide polymorphism (SNP) analysis of hiPSCs compared to their parental skin fibroblast cells was used to confirm genome integrity after reprogramming. DNA was extracted from somatic and hiPSC samples using the QIAGEN QiaAmp kit, according to the manufacturer's recommendations. The gDNA was quantified using a nanodrop. 200 ng of gDNA was outsourced to Integrigen Company (Evry, France) for karyotype analysis using HumanCore-24-v1 SNP arrays. This array contains over 300,000 probes distributed throughout the genome with a median coverage of one probe every 5700 bases. All genomic positions were based on Human Genome Build 37 (hg19). Analysis was performed with GenomeStudio software. Chromosome abnormalities were determined by visual inspection of logR ratios and B-allele frequencies (BAF) values and comparing parental cells and hiPS-derived samples. LogR ratio, the ratio between observed and expected probe intensity, is informative of copy number variation (CNV, *i.e.*, deletions/duplications), whereas BAF is informative of heterozygosity. SNP data was used to compute CNV. In particular, this type of chips allows detecting loss of heterozygosity (LOH), an important concern for hiPSC, which is not detectable with classical CGH arrays.

2.4 Differentiation of hiPSCs into cardiomyocytes (CMs)

At 80% of cell confluency, hiPSC lines were passaged using Gentle Cell Dissociation Reagent (STEMCELL Technologies) and Y-27632 Rho-kinase inhibitor (STEMCELL Technologies). The matrix sandwich method was used to generate CMs, as previously described [13]. From day 5 of differentiation, cell media was changed every other day with RPMI-1640 medium supplemented with B27 (with insulin; Thermo Fisher Scientific). After 20 to 28 days following the beginning of differentiation, spontaneously beating cell clusters were mechanically isolated using a needle and then used for electrophysiological, biochemical and molecular analyses.

2.5 RNA expression

RNA extraction: Samples of total RNA were obtained using the NucleoSpin RNA kit (MACHEREY-NAGEL) following manufacturer's specifications.

TaqMan low-density array (TLDA) : TLDA studies were conducted using six ventricular and six atrial control murine tissues as well as beating clusters of hiPS-CMs obtained from 12 control and 9 *IRX5*-mutant CM differentiations. 1µg of RNA was reverse transcribed into cDNA using SuperScript IV Vilo Master Mix (Thermo Fisher Scientific). For murine tissues, three specifically designed 384-well TLDA were used: one containing 4x 96 primers and probes for cardiac ion channels [11] and 2 others, each containing a set of 4x 96 primers and probes for cardiac transcription factors (Supplemental Table 2A). For hiPS-CMs, TLDA probe selection covered gene families implicated in cardiac ion channel expression and regulation, and cardiomyocyte structure (Supplemental Table 2B). Genes with average Ct > 32 in all compared groups were considered undetectable and excluded from the analysis (*SCN10A* and *ABCC8*). Average Ct of remaining genes for each sample was used for data normalization [14–16].

3' Sequencing RNA Profiling (3'SRP): 3'SRP protocol was performed according to Kilens et al [17]. Briefly, the libraries were prepared from 10 ng of total RNA. 40 RNA samples were extracted from 8 *IRX5*-mutated and 13 control hiPSC samples (a duplicate for each clone obtained at different cell passages) and 19 samples of corresponding hiPS-CMs. The mRNA poly(A) tail was tagged with universal adapters, well-specific barcodes and unique molecular identifiers (UMIs) during template-switching reverse transcriptase. Barcoded cDNAs from multiple samples were then pooled, amplified and tagged using a transposon-fragmentation approach which enriches for 3'ends of cDNA. A library of 350-800bp was run on an Illumina HiSeq 2500 using a HiSeq Rapid SBS Kit v2 (50 cycles; FC-402-4022) and a HiSeq Rapid PE Cluster Kit v2 (PE-402-4002). Read pairs used for analysis matched the following criteria: all

sixteen bases of the first read had quality scores of at least 10 and the first six bases correspond exactly to a designed well-specific barcode. The second reads were aligned to RefSeq human mRNA sequences (hg19) using bwa version 0.7.4 4. Reads mapping to several positions into the genome were filtered out from the analysis. Digital gene expression profiles were generated by counting the number of unique UMIs associated with each RefSeq genes, for each sample. R package DESeq2 was used to normalize gene expression. Differentially expressed genes were finally clustered using cluster 3.0 software. Enriched biological pathways were assigned for differentially expressed genes in *IRX5*-mutated vs. control hiPS-CMs. For that, Reactome pathways were attributed to the most variant genes with p-value <0.05 [18,19]. However, genes encoding for ion channels exhibited low expression levels and therefore they were not taken into consideration for differentially expressed genes analysis. To overcome this issue, p-values for these genes were calculated based on TLDA analysis. Babelomics was then used to calculate enrichment of Reactome pathways for genes differentially expressed in both TLDA and 3'SRP analyses. Finally, enrichment scores (ES) were calculated [20,21].

2.6 Protein expression and interaction

Protein extraction: *IRX5*, Nav1.5, Cx40 and GATA4 expression were evaluated in human left and right ventricular tissues obtained from three non-diseased individuals as previously described [22]. Corresponding sub-endocardial and sub-epicardial tissue slices were obtained at the cardiac base and snap-frozen in liquid nitrogen. Protein expressions and interactions were also investigated in beating hiPS-CMs at day 28 of differentiation. For protein extraction, cells were homogenized on ice using lysis buffer containing in mM: 1% TritonX-100; 100 NaCl; 50 Tris-HCl; 1 EGTA; 1 Na₃VO₄; 50 NaF; 1 phenylmethylsulfonyl fluoride and protease inhibitors cocktail (P8340, Sigma-Aldrich). Extracted samples were sonicated and centrifuged at 15,000 × g for 15 min at 4°C. Protein quantification was carried out using Pierce™ BCA Protein Assay Kit (Thermo Fisher).

Subcellular protein fractionation: To unveil the impact of *IRX5* mutations on its cellular localization, nuclear and cytosolic proteins were separated. For that, cytoplasmic membranes were disrupted on ice in a hypotonic solution including in mM: 500 HEPES, 500 MgCl₂, 500 KCl, 0.1 DTT and protease inhibitor cocktail. Cells nuclei were pelleted by 2000 rpm centrifugation and the supernatant contained the cytosolic fraction. In order to extract nuclear proteins, a protein extraction buffer was added to pellets followed by sonication.

Co-immunoprecipitation: This was performed to investigate protein-to-protein interactions between *IRX5* and GATA4 in hiPS-CMs. A total of 12.5 µl magnetic Dynabeads® Protein G

(Thermo Fisher Scientific) were added to 3 µg anti-IRX5 antibody (WH0010265M1, Sigma-Aldrich) or anti-mouse IgG antibody as control (02-6502, Thermo Fisher Scientific) and conjugated by incubation for 40 min at room temperature with rotation. The complex beads-antibody was cross-linked using 27 mg DMP (dimethyl pimelimidate, Thermo Fisher Scientific), and then incubated for 2 hours with 800 µg of total lysate at 4°C. The supernatant was then discarded and the beads were washed with the lysis buffer. Proteins were eluted in 30 µl of a mixture of NuPAGE® Sample Reducing Agent (10X) and LDS Sample Buffer (4X) (Invitrogen) and heated at 60°C. The samples were then loaded onto a 4-15% precast polyacrylamide gel (Bio-Rad).

2.7 Immunofluorescence

HiPSCs or hiPS-CMs at day 20 of differentiation were dissociated using collagenase II (Gibco) and seeded onto 8-wells iBidi plates (Biovalley) coated with Matrigel (Corning). Twelve days later, cultured cells were immunostained using a staining buffer set according to the manufacturer's instructions (00-5523-00, Thermo Fisher Scientific). HiPS-CMs were labeled by cardiac differentiation markers, *i.e.*, Troponin I (Santa Cruz) and Troponin T (Abcam) together with either cardiac conduction actors, *i.e.*, Nav1.5 (Cell signaling), Cx40 (Santa Cruz) and Cx43 (Sigma) or transcription factor, *i.e.*, IRX5 (Sigma-Aldrich). DNA was highlighted using DAPI and pictures were taken using confocal microscopy (Nikon; MicroPICell core facility).

2.8 Chromatin immunoprecipitation (ChIP)

IRX5 binding sites: Promoter DNA sequences were found using Ensembl. Consensus sequences known to mediate Iroquois transcription factor interaction with DNA [23–25] were screened on gene promoters. Each site was verified for its conservation among species using rVista 2.0. Primers surrounding the identified conserved potential binding sites (BS) were designed using Primer 3. Corresponding primer sequences are detailed in Supplemental Table 3.

ChIP: At day 28 of differentiation, beating cardiomyocyte clusters were isolated and crosslinked. After chromatin sonication, IRX5 antibody was added followed by the addition of protein G-coated dynabeads. Following an overnight incubation, the chromatin was then eluted and reverse-crosslinked. SYBER green qRT-PCR method was finally performed using the designed primers (Supplemental Table 3) to test for enrichment of the targeted sequences. Results are shown as percentage of input.

2.9 Cellular electrophysiology

Cell dissociation: hiPS-CMS were enzymatically dissociated into single cells using collagenase II (Gibco) at 37°C for 20 min. Cells were then incubated at RT for 30 min in Kraft-Bruhe solution containing (in mM): 85 KCl; 30 K₂HPO₄; 5 MgSO₄; 20 glucose; 20 taurine; 5 Na pyruvate; 5 creatine; 2 K₂-ATP; 1 EGTA; pH 7.2 adjusted with KOH. Single cells were then plated at low density on Matrigel-coated Petri-dishes (Nunc) and recorded 11 to 14 days after dissociation.

Data recording and analysis: Stimulation and data recording were performed at 37°C using an Axopatch 200B amplifier controlled by Axon pClamp 10.6 software through an A/D converter (Digidata 1440A) (all Molecular Devices). Data were analyzed using Clampfit 10.6 software. For all cell lines, data were collected from at least 3 independent differentiations. Experimental details regarding solutions composition are described in Supplemental Table 4.

Current clamp: Action potential (AP) recordings were obtained using the amphotericin-B-perforated patch-clamp technique. Patch pipettes were pulled from borosilicate glass capillaries (Sutter instruments) to obtain a tip resistance of 2 to 3 MΩ were utilized. APs were first recorded from spontaneously beating cells which were then paced by injecting a current density of 30-35 pA/pF during 1 ms, at various frequencies. Based on several parameters previously described (maximum upstroke velocity, dV/dt_{max} ; action potential duration, APD; resting membrane potential, RMP), cells were classified as either ventricular, atrial or nodal [12]. Only ventricular cells were selected for further analysis. Electronic expression of the inward rectifier potassium current, I_{K1} , was realized using dynamic patch-clamp [26]. At 2 pA/pF of *in silico* I_{K1} injection, hiPS-CM membrane resting potential was about -80 ± 10 mV. Averaged parameters were obtained from 7 consecutive APs. Both cell stimulation and injection of I_{K1} were realized by a custom-made software running on RT-Linux and a National Instrument A/D converter (NI PCI-6221) connected to the current command of the amplifier.

Voltage clamp: I_{Na} and $I_{Ca,L}$ recordings were performed in the ruptured whole-cell configuration using voltage clamp protocol as depicted in the figures. Pipettes (Sutter instruments) with 1.7-2.5 MΩ tip resistance were waxed before use to decrease pipette capacitive currents. $I_{Ca,L}$ and I_{Na} recordings were low-pass filtered at, respectively, 3 KHz and 10 KHz. Holding potentials were respectively -80 mV and -100 mV. The capacitance and series were compensated using a VE-2 amplifier (Alembic Instrument, Qc, Canada). Leak current was subtracted. Current densities were calculated by dividing the current to the membrane capacitance (C_m). Steady-state activation and inactivation curves were fitted using a Boltzmann

equation: $I/I_{max} = A / \{1.0 + \exp [(V_{1/2} - V)/k]\}$ with $k > 0$ for the activation curve and $k < 0$ for the inactivation curve.

Action potential clamp: In order to record specific currents during AP cycles, and especially during the depolarization phase, cells membrane potential was clamped according to voltage-AP-like protocols. Representative APs acquired from spontaneously beating control hiPS-CMs with ($dV/dt_{max} = 100$ V/s; $APD_{90} = 280$ ms; $RMP = -83$ mV) or without ($dV/dt_{max} = 12$ V/s; $APD_{90} = 300$ ms; $RMP = -57$ mV) *in silico* I_{K1} injection were selected. Activated sodium current during AP was measured by subtracting traces before and after adding $30 \mu M$ tetrodotoxin TTX in I_{Na} -specific intracellular and extracellular (with 130 mM NaCl concentration) solutions (Supplemental Table 4). $I_{Ca,L}$ was considered as the Nifedipine-sensitive ($4 \mu M$) calcium current recorded using $I_{Ca,L}$ solutions (Supplemental Table 4).

2.10 Luciferase assay

SCN5A BS2- (from -261 to $+613$ bp of the TSS) and BS2+ (from -261 to $+1072$ bp from TSS) Plasmids (150 ng), pGL2-Renilla (15 ng) with or without GATA4 expressing vector (150 ng) and with or without either of the wild-type or mutated forms of *IRX5* expressing vectors (150 ng) were transfected into HEK293 cells using Lipofectamine 2000 (Thermo Fisher Scientific). DNA quantities were equalized in each condition using empty pcDNA3.1. Cells were harvested 48 hours later and luciferase activity was measured using Dual Luciferase reporter assay system (Promega).

2.11 Microscale Thermophoresis (MST)

MST was used to verify protein interaction with DNA according to Nanotemper instructions. Briefly, HEK293 cells transfected by *IRX5-GFP* expressing vector were used to produce fluorescently labeled *IRX5* protein. Cell lysates were prepared using a buffer containing 20 mM Tris HCl, 130 mM NaCl, 1% NP40 and protease inhibitors cocktail. Titration series were performed to obtain varying concentrations of *SCN5A* plasmids. Measurements were accomplished in standard treated capillaries on Monolith NT.115 instrument using 80% of laser power.

2.12 Statistical analysis

Results are expressed as mean \pm SEM. Comparisons were made by use Student *t*-test, or two-way ANOVA with Bonferroni post-hoc test for repeated measures. Values of $p < 0.05$ were considered statistically significant. Statistical analyses were performed with GraphPad Prism software.

3. Results

3.1 *IRX5* TF expression correlates with conduction genes expression in human cardiac tissues

In order to identify evolutionary-conserved *IRX5*-coregulated genes in contractile tissues, expression profiles of cardiac genes including ion channels and TFs were compared between murine and human tissues. Overall, the global gene expression contrast profile between atrial and ventricular murine tissues were conserved in human samples (Figure 1A). The cluster of genes that are more expressed in ventricular tissues, included *IRX5* and several genes involved in cardiac conduction, such as *SCN5A*, which encodes the main cardiac sodium channel $\text{Na}_v1.5$ (Figure 1A). Then, the correlations between *IRX5* gene expression level and those of sodium channels and connexins (Cx), the two main families of genes implicated in cardiac conduction in humans, were investigated in the ventricles. Interestingly, *SCN5A* and *GJA5*, encoding one of the main cardiac Cx, Cx40, showed the strongest correlations with *IRX5* (Figure 1B). In accordance with these results and confirming previous results concerning *IRX5* human protein expression [22], both $\text{Na}_v1.5$ and Cx40 shared a gradient of protein expression similar to that of *IRX5* throughout the human ventricular wall with a higher level in sub-endocardium as compared to sub-epicardium (Figure 1C).

Taken together, these analyses shed light on the importance of studying the role of *IRX5* in the regulation of cardiac ventricular genes, and more specifically in the regulation of players of cardiac electrical conduction in human ventricles. The analysis of the role of *IRX5* in humans was then pursued using hiPSCs obtained from three non-diseased individuals (shown as averaged) as well as from two patients carrying different loss-of-function (LOF) mutations in *IRX5* gene associated to a QRS prolongation on the ECG (Figure S1A) [7].

3.2 *IRX5*-mutated hiPS-CMs derived from HMMS patients are a relevant model to study *IRX5* role.

Dermal fibroblasts of two homozygous carriers of either the A150P- or the N166K-*IRX5* mutation [7] and of 3 intra- and extra-familial control subjects were reprogrammed into hiPSCs. Mutations were confirmed by sequencing in hiPSCs (Figure S1B). Genome integrity was validated using SNP analysis (data not shown). Expression of pluripotency markers was verified in hiPSCs (Figure S1C-E).

We then investigated whether all hiPSC lines differentiated in a comparable manner. Principal Component Analysis (PCA) of individual transcriptomic profiles as well as correlation analysis

showed that samples mainly clustered according to their differentiation stage (Figure 2A and 2B). Furthermore, all control and *IRX5*-mutated hiPS-CMs presented a similar global change in gene expression compared to that of hiPSCs (Figure 2C). These data showed that all hiPSCs, irrespectively of their genetic background, differentiated similarly into cardiac cells. Immunostaining analysis showed that striated Troponin I was present in CMs derived from each hiPSC line (Figure 2D). Moreover, the proportions of nodal-like, atrial-like and ventricular-like cells identified using patch-clamp were comparable in control and mutated hiPS-CMs, with the ventricular-like type forming the majority of hiPS-CMs (Figure 2E). Altogether, these data confirmed that control and *IRX5*-mutated hiPSCs differentiated similarly into cardiomyocytes, and therefore that hiPS-CMs are a relevant model to investigate the role of *IRX5* in ventricular electrical conduction.

Regarding the impact of *IRX5* mutations on its own expression, transcriptional analysis and nuclear protein expression revelation showed comparable *IRX5* expression levels in control and *IRX5*-mutated hiPS-CMs (Figure 2F-2G). Finally, immunostainings of hiPS-CMs constantly showed localization of *IRX5* in CM nuclei (Figure 2D). These data showed that A150P and N166K mutations neither alter *IRX5* expression nor its localization in hiPS-CMs.

3.3 Key cardiac electrical conduction gene expression depends on *IRX5*

Global transcriptomic analysis in hiPS-CMs, using 3'SRP, unveiled 745 genes differentially expressed between control and *IRX5*-mutated cells, including several cardiac electrical conduction genes (Figure 3A). Using high-throughput real-time RT-PCR (TLDA) we also analyzed a set of 96 genes, including mostly genes with low expression level that could not be properly detected using 3'SRP (Figure 3B). Overall, for the genes detected with both techniques, expression profiles were concordant (Figure S2). Biological pathway enrichment analysis revealed that differentially expressed genes were enriched in muscle contraction pathway, and more specifically in the cardiac conduction and phase 0 AP-depolarization functions, mainly linked to the activity of *SCN5A* and *GJA5* (Figure 3C). More precisely, analyses of *IRX5*-A150P and -N166K hiPS-CMs concordantly showed major mRNA and protein expression reductions of both *SCN5A* and *GJA5* (Figure 4A-4B). Also, confocal microscopy further confirmed that *Nav1.5* and *Cx40* expression was decreased in troponin T positive *IRX5*-A150P and -N166K mutated hiPS-CMs (Figure 4C). In accordance with the delayed conduction in HMMS patients, mRNA and protein levels of *Cx43*, which has a lower conductance than *Cx40*, were increased in both mutated hiPS-CMs, with an apparent

abnormally cytoplasmic localization, suggesting that this increase in Cx pool may not be functional (Figure S3).

Taken together, hiPS-CMs carrying *IRX5* LOF mutations, exhibited altered expression of key genes involved in cardiac electrical conduction, suggesting a role for *IRX5* in the direct transcriptional control of these genes.

3.4 AP depolarization and I_{Na} density are modulated by *IRX5*

Given the delayed ventricular conduction phenotype observed in HMMS, a slower AP depolarization in patient-derived hiPS-CMs was expected. However, the depolarization velocity (dV/dt_{max}) of ventricular APs, was not statistically reduced in *IRX5*-mutated hiPS-CMs (Figure 5A). Therefore, we hypothesized that this could be due to low I_{K1} density, as recorded cellular resting membrane potentials (RMPs) of all hiPS-CMs were at about -60mV (Figure 5B), that may not be suitable for proper activation of depolarizing currents. To overcome this issue, an *in-silico* I_{K1} injection was performed. It brought ventricular RMPs to about -80mV (Figure 5B) and revealed a significant reduction in dV/dt_{max} in *IRX5*-mutated hiPS-CMs (Figure 5C). The contribution of I_{Na} and $I_{Ca,L}$ to AP depolarization was then investigated. They were measured when ventricular-like AP voltages, recorded with or without I_{K1} injection, were applied to control hiPS-CMs. Without I_{K1} injection, $I_{Ca,L}$ contribution to the depolarization phase was greater than that of I_{Na} , while with I_{K1} injection, I_{Na} became the main contributor (Figure 5D). This suggests that the dV/dt_{max} reduction observed in *IRX5*-mutated hiPS-CMs under I_{K1} injection was due to a functional reduction of I_{Na} , but not of $I_{Ca,L}$. Confirming this hypothesis, I_{Na} was reduced by half in *IRX5*-mutated hiPS-CMs (Figure 5E and Figure S4A) without any change in the (in)activation kinetics (Figure S4B and Supplemental Table 5). In contrast to I_{Na} reduction, no modification in $I_{Ca,L}$ density was observed (Figure 5F). Together with the *SCN5A* expression alteration, these data suggest that a slower ventricular AP depolarization due to I_{Na} reduction may participate to the prolonged QRS observed in HMMS.

3.5 *IRX5* interacts with *SCN5A*, *GJA5* and *GJA1* promoters

Considering the altered transcription of *Cx* and *SCN5A* induced by *IRX5* LOF, we explored whether *IRX5* regulates directly their promoters. An *in-silico* analysis showed that *SCN5A* promoter region includes three potential TF-binding sites (BS) for *IRX5* (Figure 6A). In accordance with previous studies on mice [9], human *GJA5* promoter region was free from any conserved *IRX* BS (Figure 6B) while *GJA1* promoter contained 2 conserved *IRX* BSs (Figure 6C). Immunoprecipitation of *IRX5*-associated chromatin showed an enrichment of *SCN5A*-BS2

in control hiPS-CMs, revealing an interaction with IRX5, but not in *IRX5*-mutated hiPS-CMs (Figure 6A). On the other hand, despite the absence of *in-silico* identification of conserved *IRX*-*BS* on *GJA5* promoter, an interaction between IRX5 and *GJA5* core promoter was found in control hiPS-CMs, that was again absent in *IRX5*-mutated hiPS-CMs (Figure 6B). Finally, binding of IRX5 was detected on *GJA1-BS1* in control hiPS-CMs that was again not observed in *IRX5*-mutated iPS-CMs (Figure 6C). These data strongly suggest that IRX5 interacts with *SCN5A*, *GJA5*, and *GJA1* promoters to regulate their expression in hiPS-CMs.

To further investigate the direct interaction between *SCN5A* promoter and IRX5, their binding affinity was evaluated. Two different DNA constructs containing *SCN5A* promoter were used: BS2+ plasmid, containing *IRX5 BS2* and BS2- plasmid, lacking *IRX5 BS2*. Interestingly, IRX5 protein did bind to BS2+ plasmid but not to BS2- plasmid, confirming that IRX5 protein binds to *SCN5A* promoter when BS2 is present (Figure 6D).

Finally, the functional consequences of IRX5 binding on *SCN5A* promoter were further evaluated using luciferase assay with the BS2+ plasmid construct. Unexpectedly, neither IRX5 nor its mutated forms activated the *luciferase* reporter gene (Figure 6E), indicating that another TF may be required to allow IRX5 to regulate *SCN5A* expression. This prompted us to investigate the role of potential critical partners for IRX5, already known to be important for regulation of cardiac development and electrical function, such as GATA4. GATA4, a cardiogenic TF, has indeed been previously shown to regulate *SCN5A* expression [27] and an interaction between *Irx5* and another member of the Gata family of TFs, *Gata3*, has been unveiled during craniofacial development [7].

3.6 IRX5 and GATA4 cooperatively regulate *SCN5A* expression in human cardiomyocytes

Comparably in human cardiac ventricular samples and control hiPS-CMs, among GATA family members, GATA4 was the most strongly expressed (Figure 7A). In control hiPS-CMs, GATA4 co-immunoprecipitated with IRX5 and this interaction was not altered in *IRX5*-mutated hiPS-CMs (Figure 7B). As *SCN5A* promoter contains two sites for GATA4 binding (*BSa* and *BSb*) [27], ChIP experiments using IRX5 antibody showed that IRX5 interacted with *GATA4 BSb* region in control and *IRX5*-mutated hiPS-CMs (Figure 7C). Binding affinity analysis further validated the direct interaction between *SCN5A* promoter and the heterodimer IRX5-GATA4, as a binding was observed when both IRX5 and GATA4 proteins were mixed with BS2- plasmid, in opposition to when IRX5 alone was mixed with BS2- plasmid (Figure S5). Therefore, IRX5 not only binds directly to *BS2* on *SCN5A* promoter but also binds the *BSb* site together with GATA4. Finally, to further dissect the role of IRX5 and GATA4 on *SCN5A*

transcription activation, luciferase assays were performed with plasmids containing either *BSb* only (BS2- plasmid) or *BSb* and *BS2* (BS2+ plasmid). Co-transfection of GATA4 expressing vector with either plasmid triggered a similar increase in luciferase activity, confirming that GATA4 activated *SCN5A* promoter through a direct interaction with *BSb* (Figure 7D). Interestingly, when IRX5 was added to these combinations, it potentiated by 1.6 times the effect of GATA4 on BS2- plasmid, and by 3.9 times the effect of GATA4 on BS2+ plasmid (Figure 7D). This further demonstrated that the direct binding of IRX5 to *BS2* is important for proper activation of *SCN5A* expression. Conversely, no potentiation of GATA4 activation of *SCN5A* promoter was observed when A150P- or N166K-mutated IRX5 were added to the various combinations (Figure 7D). Interestingly, in contrast to *IRX5* and *SCN5A*, which shared similarly-graded expression patterns, *GATA4* was homogeneously expressed both in atria and ventricles, and throughout the ventricular wall (Figure S6A-D). This suggests that GATA4 triggers basal expression of *SCN5A* throughout cardiac tissues, while IRX5 is responsible for the establishment of its expression gradient.

4. Discussion

This study demonstrates that IRX5 TF is instrumental for proper control of electrical activity in human cardiomyocytes. Overall, the present data suggest that the specific ventricular transmural expression pattern of IRX5 is essential for graded regulation of sodium channel- and connexin-gene expression, ensuring coordinated conduction of the electrical influx through the ventricles.

4.1 HiPSCs as a model to study TFs

It is commonly acknowledged that stem cell-derived cardiomyocytes fail to recapitulate adult CM features [28]. Nevertheless, hiPS-CMs have been used successfully so far in more than 35 studies of cardiac arrhythmic diseases and channelopathies [28]. Recently, 2 studies showed the role of TFs in cellular dysfunction associated to cardiac morphogenetic and electrical defects using hiPS-CMs [29,30]. The present work additionally enforces the use of hiPSCs as a relevant model for studying the role of TF in the regulation of cardiac electrical conduction. Indeed, with *in-silico* I_{K1} injection, we revealed cellular phenotypic traits that are consistent with the patient's clinical phenotype, *e.g.* QRS complex prolongation observed on the patient's ECG.

4.2 Interspecies regulatory pathway differences

Electrophysiological properties across species are known to be different [31], suggesting that the roles of cardiac TFs can differ from one species to another. Here, in agreement with this postulate, comparably to what was previously demonstrated for *Irx3* and its regulation of fast conduction in the murine heart [9], a direct repression of *GJA1* and indirect induction of *GJA5* by IRX5 has been described in human iPS-derived cardiomyocytes. However, *Irx5*KO mice did not exhibit conduction delay and murine *Irx5* was not found to regulate the expression of *Cx* [32].

Moreover, the patients, unlike *Irx5*KO mice, do not display ventricular repolarization abnormalities, but a conduction defect. Indeed, the deletion of *Irx5* in mice leads to the abolishment of the T wave on the ECG due to the loss of the transmural gradient of expression of *Kcnd2*, at the root of one major player of ventricular repolarization in mice, I_{to} , but not in human heart, where *KCND3* constitute the predominant alpha-subunit generating I_{to} [22]. Another argument in favor of interspecies differences in gene regulation by IRX TFs is that, due to its transmural gradient of expression, *Irx5* establishes gradients of expression for its target genes. That is how, in mice, *Kcnd2* ventricular gradient is known to be established. In

human, it is unlikely that *IRX5* regulates *KCND3* expression, as, in opposition to *IRX5*, its expression is uniform across the ventricular wall [8,22].

Along with this rationale, in this study, using patient-derived cardiomyocytes, a role for *IRX5* in the regulation of the expression of the major actors of conduction of the electrical influx, sodium channel subunit and connexins, was elucidated. These data illustrate interspecies differences in the mechanism of action of Iroquois TFs, demonstrating the importance of using appropriate models to study human diseases.

4.3 Complex regulatory pathway underlies electrical conduction

Conduction of electrical influx throughout the ventricles is mediated not only by connexins but also by inward currents responsible for the depolarization phase of APs. Here, among these inward currents (I_{Na} and $I_{Ca,L}$), I_{Na} reduction has been identified as the trigger of the impaired AP upstroke velocity in mutated hiPS-CMs. In agreement, *IRX5* binds to and activates *SCN5A* proximal promoter in control hiPS-CMs whereas mutations in *IRX5* prevent this interaction. Surprisingly, at the functional level, luciferase assays showed that *IRX5* alone was not able to activate *SCN5A*, suggesting that regulation of *SCN5A* is due to a combinatorial effect of several factors. In accordance, *IRX5* and *GATA4* have been found to interact with each other allowing *IRX5* to bind to a previously described *GATA4* BS on *SCN5A* promoter and to enhance *GATA4* effect on *SCN5A* activation. Interestingly, while *IRX5* and *SCN5A* display a comparable gradient of expression through the ventricular wall, as well as a between atria and ventricles, *GATA4* has a more uniform pattern of expression. We thus hypothesized that *GATA4* and *IRX5* could act cooperatively where *GATA4* may be important for basal expression of *SCN5A* in human cardiomyocytes while *IRX5* creates its gradients of expression in the heart. Genetic expression and/or function abnormalities of *SCN5A* together with conduction defects, have been previously linked to other rare arrhythmic diseases, such as Brugada syndrome [33,34]. Thus, the current study elaborating the role of *IRX5* in the control of ventricular conduction through the regulation of *SCN5A* presents a framework for future studies on its potential implication in other complex disease such as Brugada syndrome.

4.4 Study limitations

Arrhythmic diseases often present with a wide spectrum of phenotypes, even among patients belonging to the same family. The individual genetic background is thought to play a major role in this heterogeneity. In the context of hiPSC-based disease modeling, the use of isogenic control, where the genetic variant has been corrected in the patient iPS cell line, is increasingly

employed. The present study aimed at dissecting *IRX5* regulatory mechanisms of human cardiac electrical function by modeling HMMS. Therefore, we chose to perform a comparative analysis between control and two hiPSC lines obtained from two HMMS patients belonging to different families and harboring different LOF mutations in *IRX5*. For all studied parameters, similar results have been obtained for both types of mutated hiPS-CMs as compared to control cells, strongly supporting a specific role for *IRX5* in the pathological phenotype and thereby minimizing the relevance of using isogenic controls.

5. Conclusion

In conclusion, hiPS-CMs generated from patients with rare mutations in *IRX5* recapitulated their clinical features of ventricular depolarization delay. Furthermore, a role for this transcription factor in the orchestration of the gene expression program governing ventricular electrical depolarization in human, was uncovered, bringing to light a new potential option for therapeutic intervention.

Acknowledgments:

The authors would like to thank the Genomics and Bioinformatics Core Facility (GenoBiRD, Biogenouest), the Cytometry facility (CytoCell), the iPS core facility, and the Cellular and Tissular Imaging Core Facility (MicroPICell) of Nantes University, for their technical support. The authors also would like to thank Dan Roden for the gift of SCN5A plasmids, and Sophie Demolombe for helping with mouse studies.

Sources of Funding:

This work was funded by grants from The National Research Agency [HEART iPS ANR-15-CE14-0019-01], and *La Fédération Française de Cardiologie*. Nathalie Gaborit was laureate of fellowships from Fondation Lefoulon-Delalande and International Incoming Fellowship FP7-PEOPLE-2012-IIF [PIIF-GA-2012-331436]. Zeina R. Al Sayed is supported by Eiffel scholarship program of Excellence (Campus France), by Doctoral School of Science and Technology-Lebanese University and The Fondation Genavie.

Conflict of interest: None declared.

Authors contributions:

Zeina R. Al-Sayed contributed to the acquisition, interpretation of data, and writing of the report; Robin Canac contributed to data acquisition; Bastien Cimarosti contributed to data acquisition; Carine Bonnard contributed to clinical data acquisition; Hanan Hamamy contributed to clinical data acquisition; Hulya Kayserili contributed to clinical data acquisition; Aurore Girardeau contributed to data acquisition; Mariam Jouni contributed to data acquisition; Nicolas Jacob contributed to data acquisition; Anne Gaignerie contributed to data acquisition; Caroline Chariou contributed to data acquisition; Laurent David contributed to data acquisition; Virginie Forest contributed to data acquisition; Céline Marionneau contributed to data acquisition; Gildas Loussouarn contributed to data analysis, and writing of the report; Guillaume Lamirault contributed to data analysis, and writing of the report; Bruno Reversade contributed to clinical data acquisition; Kazem Zibara contributed to the writing of the report; Patricia Lemarchand contributed to the study design, interpretation of the data, and writing of the report; Nathalie Gaborit contributed to the study design, interpretation of the data, and writing of the report. All authors discussed the results and contributed and approved the final manuscript.

References

1. Pazoki R, Wilde AAM, Bezzina CR. Genetic Basis of Ventricular Arrhythmias. *Curr Cardiovasc Risk Rep.* 2010;4:454–60.
2. Gourraud J-B, Barc J, Thollet A, Le Scouarnec S, Le Marec H, Schott J-J, Redon R, Probst V. The Brugada Syndrome: A Rare Arrhythmia Disorder with Complex Inheritance. *Front Cardiovasc Med.* 2016;3:9.
3. Van Weerd JH, Christoffels VM. The formation and function of the cardiac conduction system. *Development.* 2016;143:197–210.
4. Van Eif VWW, Devalla HD, Boink GJJ, Christoffels VM. Transcriptional regulation of the cardiac conduction system. *Nat Rev Cardiol.* 2018.
5. Hu W, Xin Y, Zhang L, Hu J, Sun Y, Zhao Y. Iroquois Homeodomain transcription factors in ventricular conduction system and arrhythmia. *Int J Med Sci.* 2018;15:808–15.
6. Hamamy HA, Teebi AS, Oudjhane K, Shegem N, Ajlouni K. Severe hypertelorism, midface prominence, prominent/simple ears, severe myopia, borderline intelligence, and bone fragility in two brothers: New syndrome? *Am J Med Genet A.* 2007;143A:229–34.
7. Bonnard C, Strobl AC, Shboul M, Lee H, Merriman B, Nelson SF, Ababneh OH, Uz E, Güran T, Kayserili H, Hamamy H, Reversade B. Mutations in IRX5 impair craniofacial development and germ cell migration via SDF1. *Nat Genet.* 2012;44:709–13.
8. Costantini DL, Arruda EP, Agarwal P, Kim K-H, Zhu Y, Zhu W, Lebel M, Cheng CW, Park CY, Pierce SA, Guerchicoff A, Pollevick GD, Chan TY, Kabir MG, Cheng SH, Husain M, Antzelevitch C, Srivastava D, Gross GJ, Hui C, Backx PH, Bruneau BG. The Homeodomain Transcription Factor Irx5 Establishes the Mouse Cardiac Ventricular Repolarization Gradient. *Cell.* 2005;123:347–58.
9. Zhang S-S, Kim K-H, Rosen A, Smyth JW, Sakuma R, Delgado-Olguín P, Davis M, Chi NC, Puvion-Vandier V, Gaborit N, Sukonnik T, Wylie JN, Brand-Arzamendi K, Farman GP, Kim J, Rose RA, Marsden PA, Zhu Y, Zhou Y-Q, Miquerol L, Henkelman RM, Stainier DYR, Shaw RM, Hui C, Bruneau BG, Backx PH. Iroquois homeobox gene 3 establishes fast conduction in the cardiac His–Purkinje network. *Proc Natl Acad Sci.* 2011;108:13576–81.
10. Kim K-H, Rosen A, Hussein SMI, Puvion-Vandier V, Korogyi AS, Chiarello C, Nagy A, Hui C, Backx PH. Irx3 is required for postnatal maturation of the mouse ventricular conduction system. *Sci Rep.* 2016;6:19197.
11. Marionneau C, Couette B, Liu J, Li H, Mangoni ME, Nargeot J, Lei M, Escande D, Demolombe S. Specific pattern of ionic channel gene expression associated with pacemaker activity in the mouse heart. *J Physiol.* 2005;562:223–34.
12. Jouni M, Si-Tayeb K, Es-Salah-Lamoureux Z, Latypova X, Champon B, Caillaud A, Runge A, Charpentier F, Loussouarn G, Baró I, Zibara K, Lemarchand P, Gaborit N. Toward Personalized Medicine: Using Cardiomyocytes Differentiated From Urine-Derived Pluripotent Stem Cells to Recapitulate Electrophysiological Characteristics of Type 2 Long QT Syndrome. *J Am Heart Assoc.* 2015;4:e002159.

- 587 13. Es-Salah-Lamoureux Z, Jouni M, Malak OA, Belbachir N, Sayed ZRA, Gandon-Renard
588 M, Lamirault G, Gauthier C, Baró I, Charpentier F, Zibara K, Lemarchand P, Beaumelle
589 B, Gaborit N, Loussouarn G. HIV-Tat induces a decrease in IKr and IKs via reduction in
590 phosphatidylinositol-(4,5)-bisphosphate availability. *J Mol Cell Cardiol.* 2016;99:1–13.
- 591 14. Wang W-X, Danaher RJ, Miller CS, Berger JR, Nubia VG, Wilfred BS, Neltner JH,
592 Norris CM, Nelson PT. Expression of miR-15/107 family microRNAs in human tissues
593 and cultured rat brain cells. *Genomics Proteomics Bioinformatics.* 2014;12:19–30.
- 594 15. Mestdagh P, Van Vlierberghe P, De Weer A, Muth D, Westermann F, Speleman F,
595 Vandesompele J. A novel and universal method for microRNA RT-qPCR data
596 normalization. *Genome Biol.* 2009;10:R64.
- 597 16. Bockmeyer CL, Säuberlich K, Wittig J, Eßer M, Roeder SS, Vester U, Hoyer PF,
598 Agustian PA, Zeuschner P, Amann K, Daniel C, Becker JU. Comparison of different
599 normalization strategies for the analysis of glomerular microRNAs in IgA nephropathy.
600 *Sci Rep.* 2016;6:31992.
- 601 17. Kilens S, Meistermann D, Moreno D, Chariou C, Gaignerie A, Reignier A, Lelièvre Y,
602 Casanova M, Vallot C, Nedellec S, Flippe L, Firmin J, Song J, Charpentier E, Lammers
603 J, Donnart A, Marec N, Deb W, Bihouée A, Caignec CL, Pecqueur C, Redon R, Barrière
604 P, Bourdon J, Pasque V, Soumillon M, Mikkelsen TS, Rougeulle C, Fréour T, David L.
605 Parallel derivation of isogenic human primed and naive induced pluripotent stem cells.
606 *Nat Commun.* 2018;9:360.
- 607 18. Croft D, Mundo AF, Haw R, Milacic M, Weiser J, Wu G, Caudy M, Garapati P,
608 Gillespie M, Kamdar MR, Jassal B, Jupe S, Matthews L, May B, Palatnik S, Rothfels K,
609 Shamovsky V, Song H, Williams M, Birney E, Hermjakob H, Stein L, D'Eustachio P.
610 The Reactome pathway knowledgebase. *Nucleic Acids Res.* 2014;42:D472–7.
- 611 19. Fabregat A, Korninger F, Viteri G, Sidiropoulos K, Marin-Garcia P, Ping P, Wu G, Stein
612 L, D'Eustachio P, Hermjakob H. Reactome graph database: Efficient access to complex
613 pathway data. *PLOS Comput Biol.* 2018;14:e1005968.
- 614 20. Medina PP, Nolde M, Slack FJ. OncomiR addiction in an in vivo model of microRNA-
615 21-induced pre-B-cell lymphoma. *Nature.* 2010;467:86–90.
- 616 21. Sartor MA, Leikauf GD, Medvedovic M. LRpath: a logistic regression approach for
617 identifying enriched biological groups in gene expression data. *Bioinforma Oxf Engl.*
618 2009;25(2):211–7.
- 619 22. Gaborit N, Varro A, Le Bouter S, Szuts V, Escande D, Nattel S, Demolombe S. Gender-
620 related differences in ion-channel and transporter subunit expression in non-diseased
621 human hearts. *J Mol Cell Cardiol.* 2010;49:639–46.
- 622 23. Biloni A, Craig G, Hill C, McNeill H. Iroquois transcription factors recognize a unique
623 motif to mediate transcriptional repression in vivo. *Proc Natl Acad Sci U S A.*
624 2005;102:14671–6.
- 625 24. Berger MF, Badis G, Gehrke AR, Talukder S, Philippakis AA, Peña-Castillo L, Alleyne
626 TM, Mnaimneh S, Botvinnik OB, Chan ET, Khalid F, Zhang W, Newburger D, Jaeger
627 SA, Morris QD, Bulys ML, Hughes TR. Variation in Homeodomain DNA Binding

- Revealed by High-Resolution Analysis of Sequence Preferences. *Cell*. 2008;133:1266–76.
25. Noyes MB, Christensen RG, Wakabayashi A, Stormo GD, Brodsky MH, Wolfe SA. Analysis of Homeodomain Specificities Allows the Family-wide Prediction of Preferred Recognition Sites. *Cell*. 2008;133:1277–89.
 26. Putten M van, E RM, Mengarelli I, Guan K, Zegers JG, Ginneken V, G AC, Verkerk AO, Wilders R. Ion channelopathies in human induced pluripotent stem cell derived cardiomyocytes: a dynamic clamp study with virtual IK1. *Front Physiol*. 2015;6:7.
 27. Tarradas A, Pinsach-Abuin M, Mackintosh C, Llorà-Batlle O, Pérez-Serra A, Batlle M, Pérez-Villa F, Zimmer T, Garcia-Bassets I, Brugada R, Beltran-Alvarez P, Pagans S. Transcriptional regulation of the sodium channel gene (SCN5A) by GATA4 in human heart. *J Mol Cell Cardiol*. 2017;102:74–82.
 28. Giacomelli E, Mummery CL, Bellin M. Human heart disease: lessons from human pluripotent stem cell-derived cardiomyocytes. *Cell Mol Life Sci CMLS*. 2017;74:3711–39.
 29. Ang Y-S, Rivas RN, Ribeiro AJS, Srivas R, Rivera J, Stone NR, Pratt K, Mohamed TMA, Fu J-D, Spencer CI, Tippens ND, Li M, Narasimha A, Radzinsky E, Moon-Grady AJ, Yu H, Pruitt BL, Snyder MP, Srivastava D. Disease Model of GATA4 Mutation Reveals Transcription Factor Cooperativity in Human Cardiogenesis. *Cell*. 2016;167:1734-1749.e22.
 30. Caballero R, Utrilla RG, Amorós I, Matamoros M, Pérez-Hernández M, Tinaquero D, Alfayate S, Nieto-Marín P, Guerrero-Serna G, Liu Q-H, Ramos-Mondragón R, Ponce-Balbuena D, Herron T, Campbell KF, Filgueiras-Rama D, Peinado R, López-Sendón JL, Jalife J, Delpón E, Tamargo J. Tbx20 controls the expression of the KCNH2 gene and of hERG channels. *Proc Natl Acad Sci*. 2017;114:E416–25.
 31. Muszkiewicz A, Britton OJ, Gemmell P, Passini E, Sánchez C, Zhou X, Carusi A, Quinn TA, Burrage K, Bueno-Orovio A, Rodriguez B. Variability in cardiac electrophysiology: Using experimentally-calibrated populations of models to move beyond the single virtual physiological human paradigm. *Prog Biophys Mol Biol*. 2016;120:115–27.
 32. Gaborit N, Sakuma R, Wylie JN, Kim K-H, Zhang S-S, Hui C-C, Bruneau BG. Cooperative and antagonistic roles for Irx3 and Irx5 in cardiac morphogenesis and postnatal physiology. *Dev Camb Engl*. 2012;139:4007–19.
 33. Gaborit N, Wichter T, Varro A, Szuts V, Lamirault G, Eckardt L, Paul M, Breithardt G, Schulze-Bahr E, Escande D, Nattel S, Demolombe S. Transcriptional profiling of ion channel genes in Brugada syndrome and other right ventricular arrhythmogenic diseases. *Eur Heart J*. 2009;30:487–96.
 34. Juang J-MJ, Tsai C-T, Lin L-Y, Liu Y-B, Yu C-C, Hwang J-J, Chen J-J, Chiu F-C, Chen W-J, Tseng C-D, Chiang F-T, Yeh H-M, Sherri Yeh S-F, Lai L-P, Lin J-L. Unique clinical characteristics and SCN5A mutations in patients with Brugada syndrome in Taiwan. *J Formos Med Assoc*. 2015;114:620–6.

Figure legends :

Figure 1: IRX5 TF and conduction genes expression in human cardiac tissues.

- A. Heatmap displaying expression level of 212 cardiac genes (ion channels and TFs) in murine atrial and ventricular tissues measured by TLDA ($-\Delta\text{Ct}$), and in human atrial and left ventricular samples (GTEx). Murine genes were clustered using hierarchical ascending method with an uncentered correlation metric and average linkage. Heatmap of the same genes was obtained in human tissues based on the murine cluster, in a supervised hierarchical manner. Yellow and blue indicate high and low expression levels respectively. Representative genes of the ventricular-specific gene cluster are listed in the yellow box.
- B. Expression level of genes encoding sodium channels and gap junction proteins in left ventricular tissues. Samples were ordered according to their IRX5 expression levels (purple gradient). Pearson correlation between each sodium channel or gap junction gene and IRX5 expression profiles are shown using pink gradients.
- C. Representative immunoblots of IRX5, $\text{Na}_v1.5$ and Cx40 levels in human protein lysates of ventricular sub-endocardial (Endo) and sub-epicardial (Epi) samples obtained from three human left (LV) and right ventricles (RV). Corresponding averaged IRX5, $\text{Na}_v1.5$ and Cx40 protein expression levels obtained from tissue samples of three individuals, normalized to Stain free.

Figure 2: Characterization of *IRX5*-mutated hiPS-cardiomyocytes

- A. Principal Component Analysis (PCA) of 21 hiPSC samples (in pink) and 19 hiPS-CM samples (in blue) based on their expression pattern of 27106 analyzed transcripts (3'SRP data).
- B. Correlation matrix of hiPSCs and hiPS-CMs expression profiles (same samples as in A). Samples were clustered using an ascending hierarchical method with Pearson as metric and ward.D2 linkage. Yellow and orange indicate high and low correlation, respectively.
- C. Heatmap showing expression levels for 9661 differentially expressed genes between hiPSCs and hiPS-CMs (same samples as in A). Genes were clustered using a hierarchical ascending method with an uncentered correlation metric and average linkage. Yellow and blue indicate high and low levels respectively.
- D. Illustrative immunostainings of IRX5 (red) and Troponin I (green) in hiPS-CMs, merged with a nuclear staining using DAPI (blue). To confirm nuclear localization of IRX5, XZ orthogonal planes are illustrated next to each picture.

- E. Representative traces and distribution (as percentage) of nodal-like, atrial-like and ventricular-like cells, based on the analysis of AP parameters in spontaneously beating hiPS-CMs.
- F. *IRX5* mRNA expression level in control and mutated hiPS-CMs at day 28 of cardiac differentiation using TaqMan® technique (Ctrl: n=22; A150P: n=8; N166K: n=14).
- G. Nuclear expression level of *IRX5* protein in control and mutated hiPS-CMs, normalized to Stain free. Representative immunoblot showing *IRX5* expression in the nuclear protein fraction (Ctrl: n=11; A150P: n=10; N166K: n=11).

Figure 3: Transcriptomic aberrations in *IRX5*-mutated cardiomyocytes.

- A. Heatmap showing hierarchical clustering of expression profiles of the 745 differentially expressed genes obtained by 3'SRP in control (Ctrl) and *IRX5*-mutated hiPS-CMs at day 28 of differentiation. 41% and 59% genes were upregulated and downregulated in *IRX5*-mutated hiPS-CMs, respectively. Yellow and blue represent high and low expression levels respectively. Relevant genes implicated in the function or regulation of cardiac electrical conduction are highlighted on the right.
- B. Histograms showing expression levels of differentially expressed genes in *IRX5*-mutated hiPS-CMs (n=9) identified using TLDA, as compared to control hiPS-CMs (n=12). * and **: p<0.05 and p<0.01 vs. control, respectively (*t* test).
- C. Top panel: Functional annotation of differentially expressed genes at day 28 of differentiation, obtained by 3'SRP and TaqMan. Histograms showing over-represented Reactome pathways. Only pathways with Enrichment Score>2 and p<0.05 are shown. Bottom panel: Detailed muscle contraction pathway is represented.

Figure 4: Impaired expression of *GJA5* and *SCN5A* in *IRX5*-mutated hiPS-CMs.

- A. TaqMan® analysis showing mRNA expression of *SCN5A* and *GJA5* in control (n=21), A150P (n=8) and N166K (n=12) *IRX5*-mutated hiPS-CMs. Cts were normalized to *ACTB* and $2^{-\Delta\Delta C_t}$ was calculated. * and **: p<0.05 and p<0.01 vs. control, respectively (*t* test).
- B. Representative immunoblots for $Na_v1.5$ and Cx40 and ratios of $Na_v1.5$ and Cx40 expression levels normalized to Transferrin receptor (TFRC). Blots were quantified using Image Lab software. ** and ***: p<0.01 and p<0.001 vs. control, respectively (*t* test). Ctrl: n=38; A150P: n=22; N166K: n=22.

C. Representative confocal images for immunostainings of Na_v1.5 and Cx40 (green) in Troponin I positive (red) control and *IRX5*-mutated hiPS-CMs. Nuclei are stained in blue using DAPI.

Figure 5: *IRX5* loss-of-function leads to a slower upstroke velocity via reduction of I_{Na}

A. Top panel: representative traces of ventricular APs measured in *IRX5*-A150P and -N166K mutated and control hiPS-CMs paced at 700ms cycle length with their corresponding first derivatives of AP upstroke velocity (arrows). Bottom panel: Box whisker plots of maximum upstroke velocities of ventricular APs when pacing at 700ms cycle length without *in-silico* I_{K1} injection.

B. Resting membrane potentials (RMPs) measured from ventricular APs paced at 700ms cycle length with or without *in-silico* I_{K1} injection. Mean and SEM are indicated; n: same as in A and C.

C. Top panel: representative traces of ventricular APs measured in A150P and N166K *IRX5*-mutated and control hiPS-CMs paced at 700ms cycle length with their corresponding first derivatives of AP upstroke velocities (arrows). Bottom panel: Box whisker plots of maximum upstroke velocities of ventricular APs when pacing at 700ms cycle length and under dynamic clamp with *in-silico* I_{K1} injection. * and **: p<0.05 and p<0.01 vs. control, respectively (*t* test).

D. Representative traces of I_{Na}-TTX-sensitive and I_{Ca,L}-Nifedipine-sensitive in control hiPS-CMs, obtained by subtraction of the current recorded before and after application of the inhibitors, when applying typical ventricular-like AP voltages, depicted on top.

E. Superimposed representative traces of I_{Na} recorded when applying the depicted voltage-clamp protocol, and mean current densities (pA/pF) vs. membrane potential (EM) recorded in hiPS-CMs. *** and #### p<0.001 vs. control for respectively *IRX5*-A150P and -N166K hiPS-CMs (Two-way Anova with Bonferroni post hoc test).

F. Superimposed representative traces of I_{Ca,L} recorded when applying the depicted voltage-clamp protocol, and mean current densities (pA/pF) vs. membrane potential (EM) obtained in hiPS-CMs.

Figure 6: *IRX5* interacts with *SCN5A*, *GJA5* and *GJA1* promoters.

A. Schematic representation of potential binding sites for *IRX5* (BS, in green; numbers indicate position referring to TSS) on *SCN5A* promoter identified *in-silico*, and PCR amplification using primers specific for each BS after hiPS-CMs chromatin immunoprecipitation (ChIP) with an antibody against *IRX5*. Results are shown as ratio of the immunoprecipitated (IPed)

DNA relative to intergenic region (IR). TSS: transcription starting site; CP: core promoter. #: $p < 0.05$ vs. IR in control samples ($n=8$); ***: $p < 0.001$ vs. control in IRX5-mutated samples; A150P $n=5$ and N166K: $n=7$ (t test).

B and C. IRX5 interaction with *GJA5* and *GJA1* promoters, respectively, obtained as in A Ctrl: $n=6$; A150P: $n=5$; N166K: $n=7$.

D. Dissociation constant (K_d) between IRX5 protein and *SCN5A* promoter obtained after microscale thermophoresis (MST) test using constant concentration of IRX5 protein and decreasing concentration of *SCN5A* promoter plasmids (from 650nM to 0.0099nM). Two different plasmids containing parts of *SCN5A* promoter were used: BS2- Plasmid, from -261 to +613bp, that did not contain *IRX5* BS2, and BS2+ Plasmid, from -261 to +1072bp, which contained *IRX5* BS2. Left panel, fitted curves issued using law of mass action. Right panel, histograms showing mean and SEM K_d ($n=3$ per group).

E. Luciferase experiments in HEK293 cells cotransfected with BS2+ Plasmid, containing *luciferase* cDNA under the control of *SCN5A* promoter region (from -261bp to +1072bp), and with expressing vectors encoding wild-type (WT), A150P or N166K-mutated *IRX5* cDNA. Firefly luciferase activity was normalized to Renilla activity (mean \pm SEM, $n=3$ per group) and is shown as ratio vs. condition without IRX5 plasmid.

Figure 7: IRX5 and GATA4 cooperate to regulate *SCN5A* expression.

A. *GATA* transcripts expression ratios vs. *GATA5* (*GATA* TF with the lowest expression). Transcript expression ratios were calculated using GTEx data for human ventricular tissues and using TLDA analysis for control hiPS-CMs. Data are expressed as mean \pm SEM.

B. Representative western blots of IRX5 and GATA4 in control and IRX5-A150P mutated hiPS-CM lysates immunoprecipitated with anti-IRX5 antibody. Quantification of the amount of GATA4 co-immunoprecipitated with IRX5, in control and, IRX5-A150P and -N166K mutated hiPS-CMs. Results are shown as ratios of the co-immunoprecipitated (IPed) GATA4 normalized to the IPed IRX5 amounts (Ctrl: $n=20$; A150P: $n=11$; N166K: $n=8$).

C. Schematic representation of *IRX5* binding site (BS; green) and *GATA4* BS (pink) on *SCN5A* promoter (numbers indicate position referring to TSS), and PCR amplification using primers specific for each BS after hiPS-CMs ChIP with an antibody against IRX5. Results are shown as ratio of the IPed DNA relative to intergenic region (IR). TSS: transcription starting site. #: $p < 0.05$ vs. intergenic region (t test). Ctrl: $n=7$; A150P $n=4$ and N166K: $n=6$.

D. Luciferase experiments in HEK293 cells cotransfected with BS2- plasmid, containing *luciferase* cDNA under the control of *SCN5A* promoter region (-261bp to +613bp) with

798 *GATA4 BSb* but not *IRX5 BS2* (white bars), or *BS2+* plasmid, containing *luciferase* cDNA
799 under the control of *SCN5A* promoter region (-261bp to +1072bp) with *GATA4 BSb* and
800 *IRX5 BS2* (green bars), and with the indicated *GATA4* or/and *IRX5* expressing plasmids.
801 Firefly luciferase activity was normalized to Renilla and is shown as ratio to its activity when
802 transfected with *SCN5A* plasmids only. ****: $p < 0.0001$ vs. condition with no *IRX5/GATA4*
803 plasmid; ### and #####: $p < 0.001$ and $p < 0.0001$ vs. condition with *GATA4* plasmid only;
804 \$\$\$: $p < 0.001$ vs. condition with *GATA4* + WT-*IRX5* plasmids (*t* test).

Figure 1

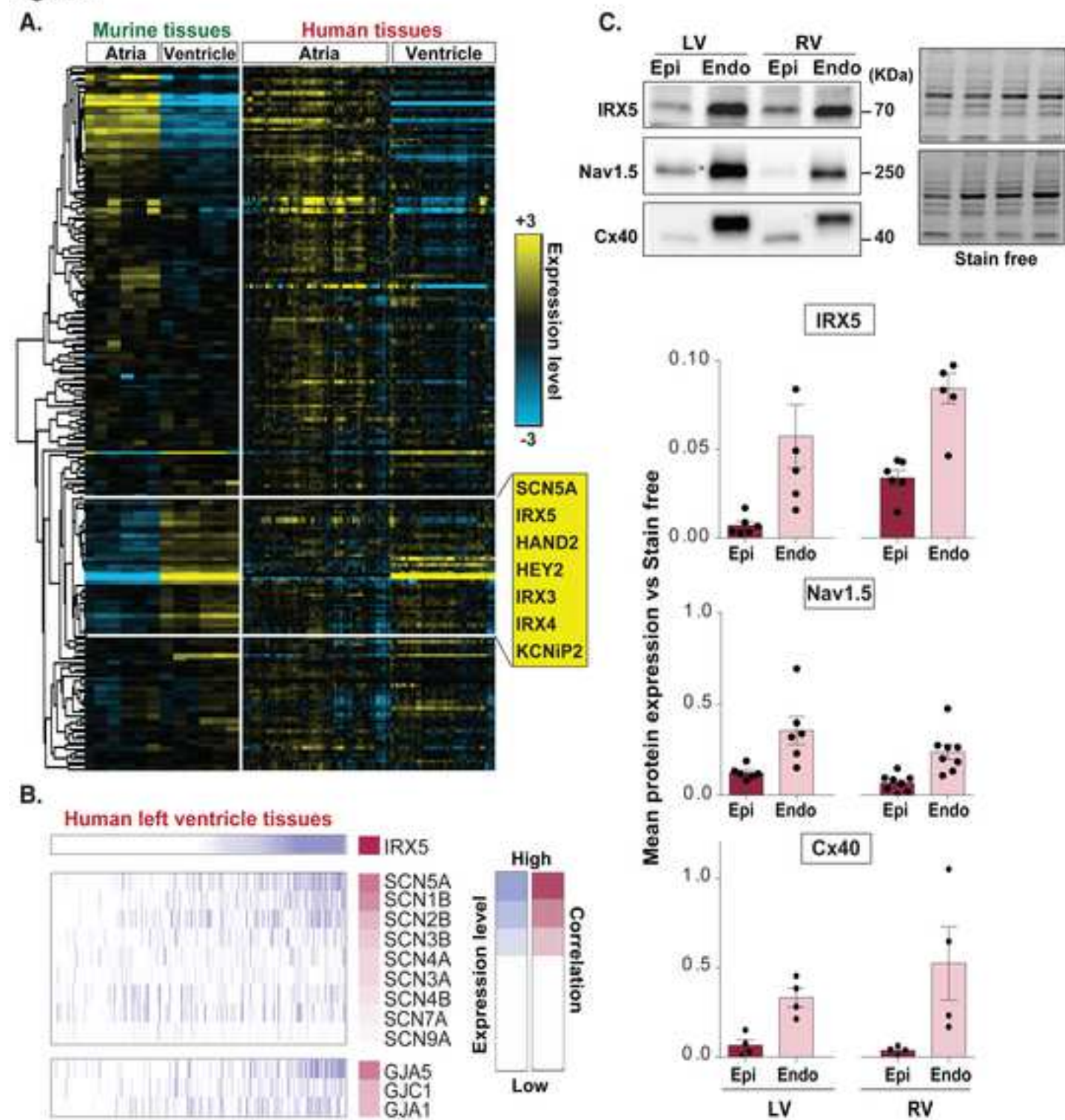


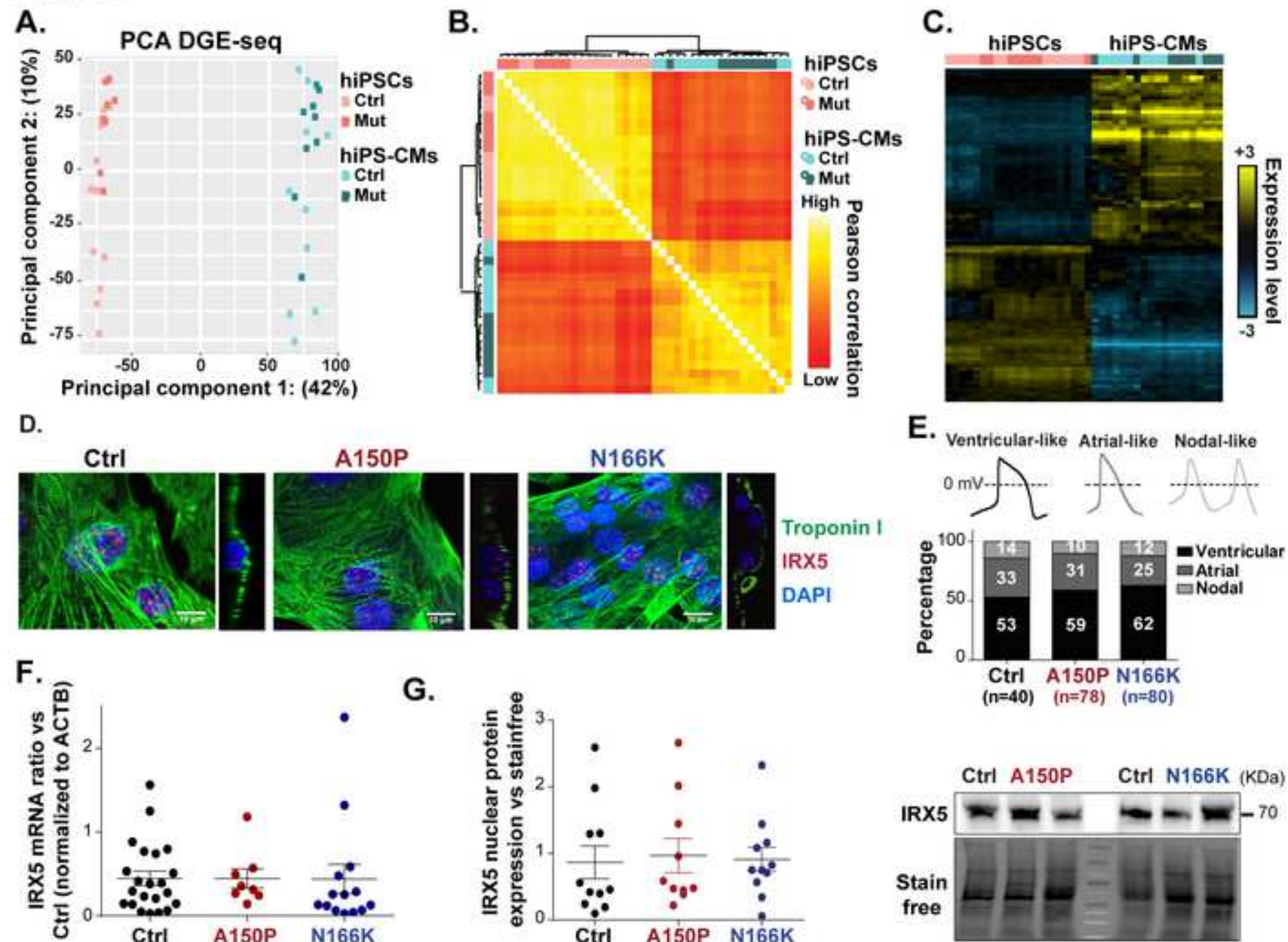
Figure 2

Figure 3

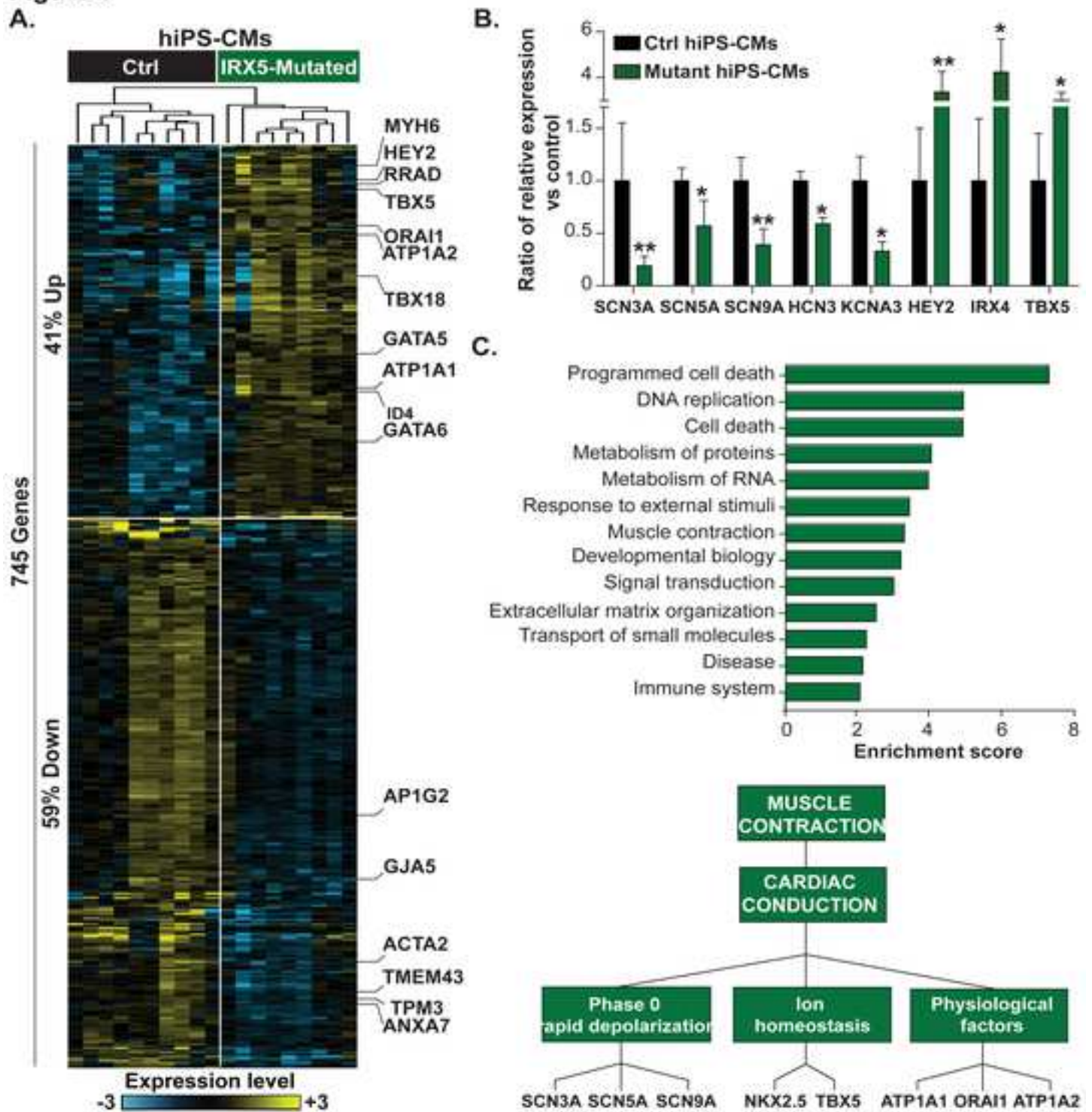


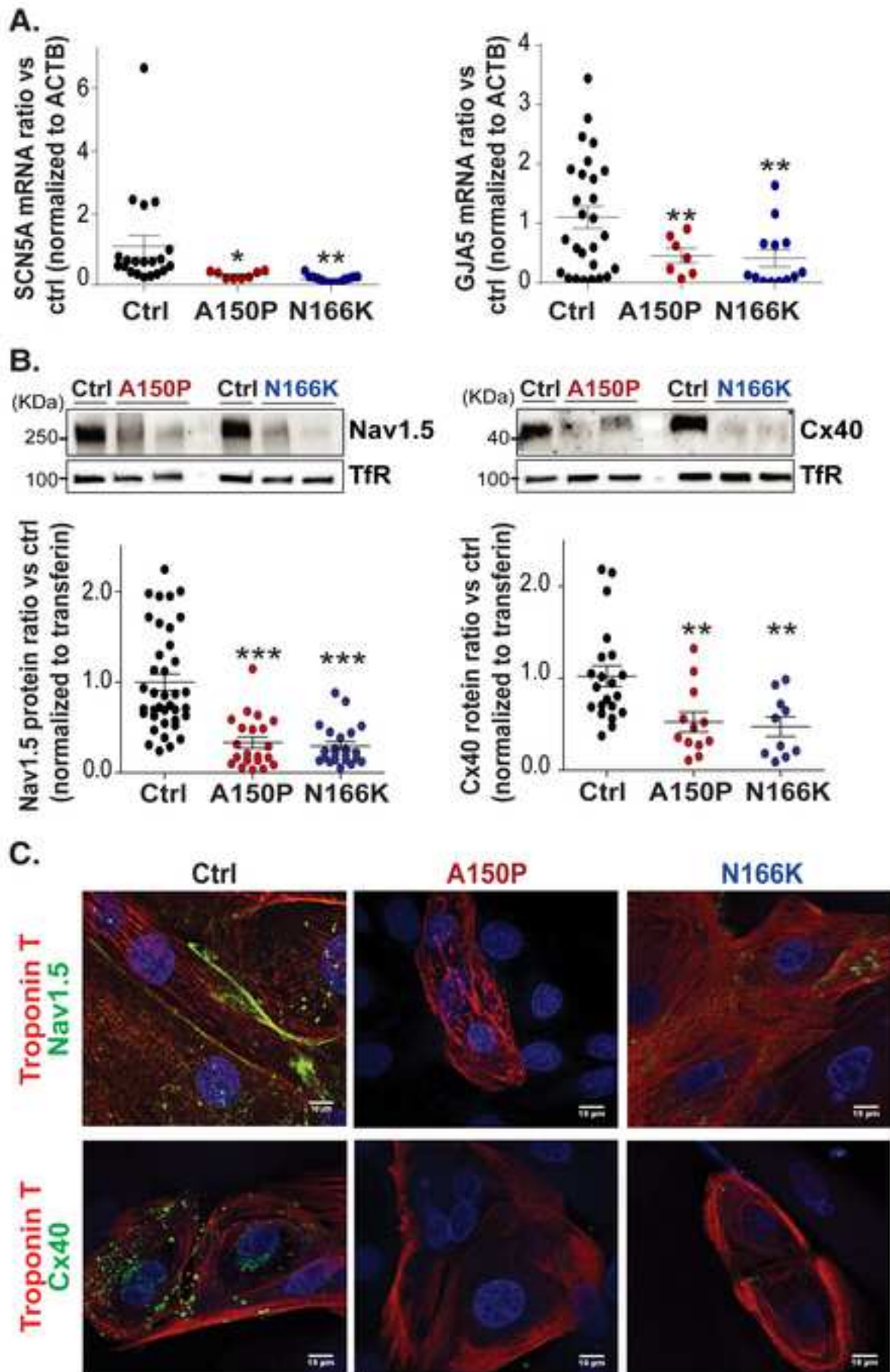
Figure 4

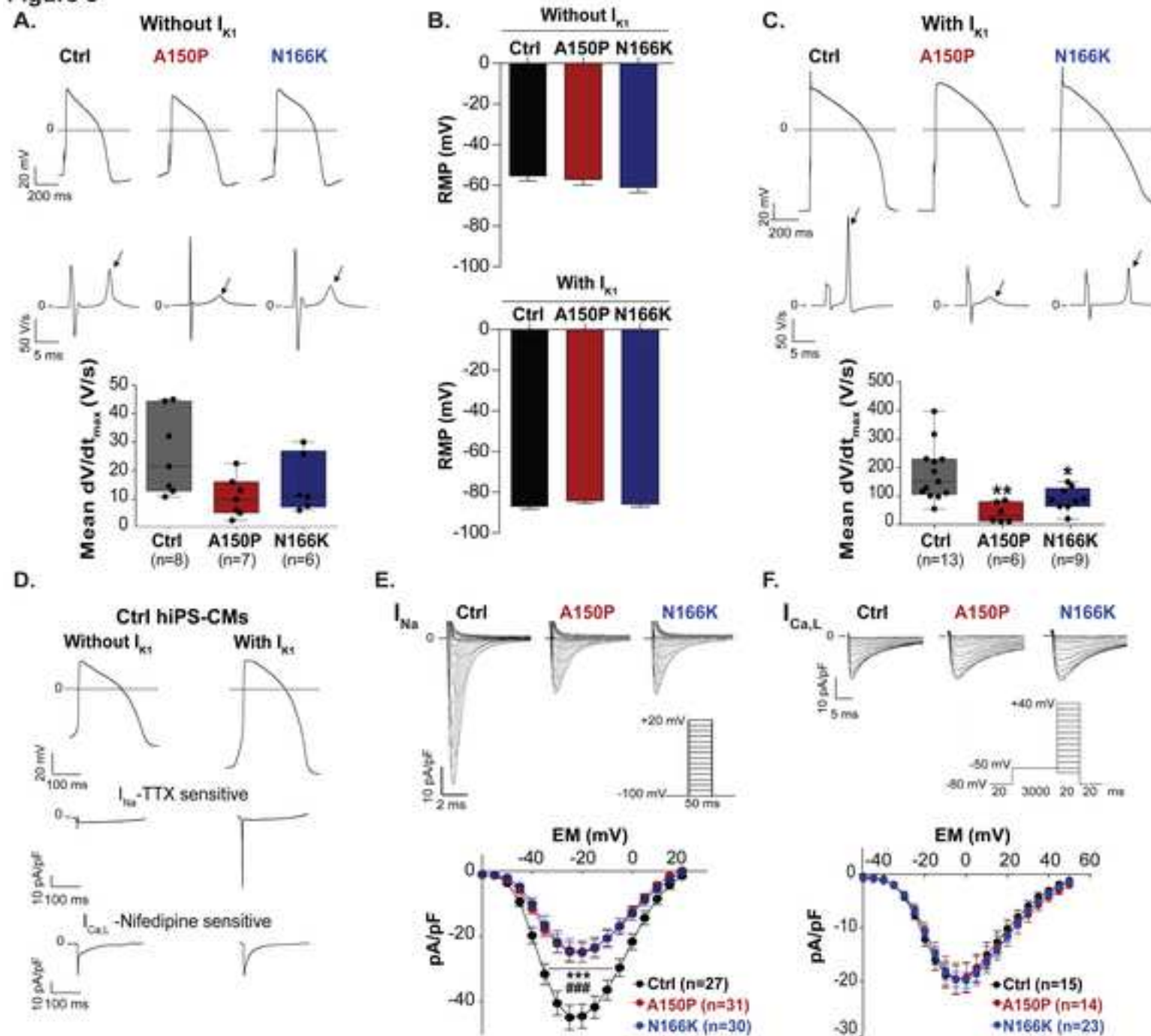
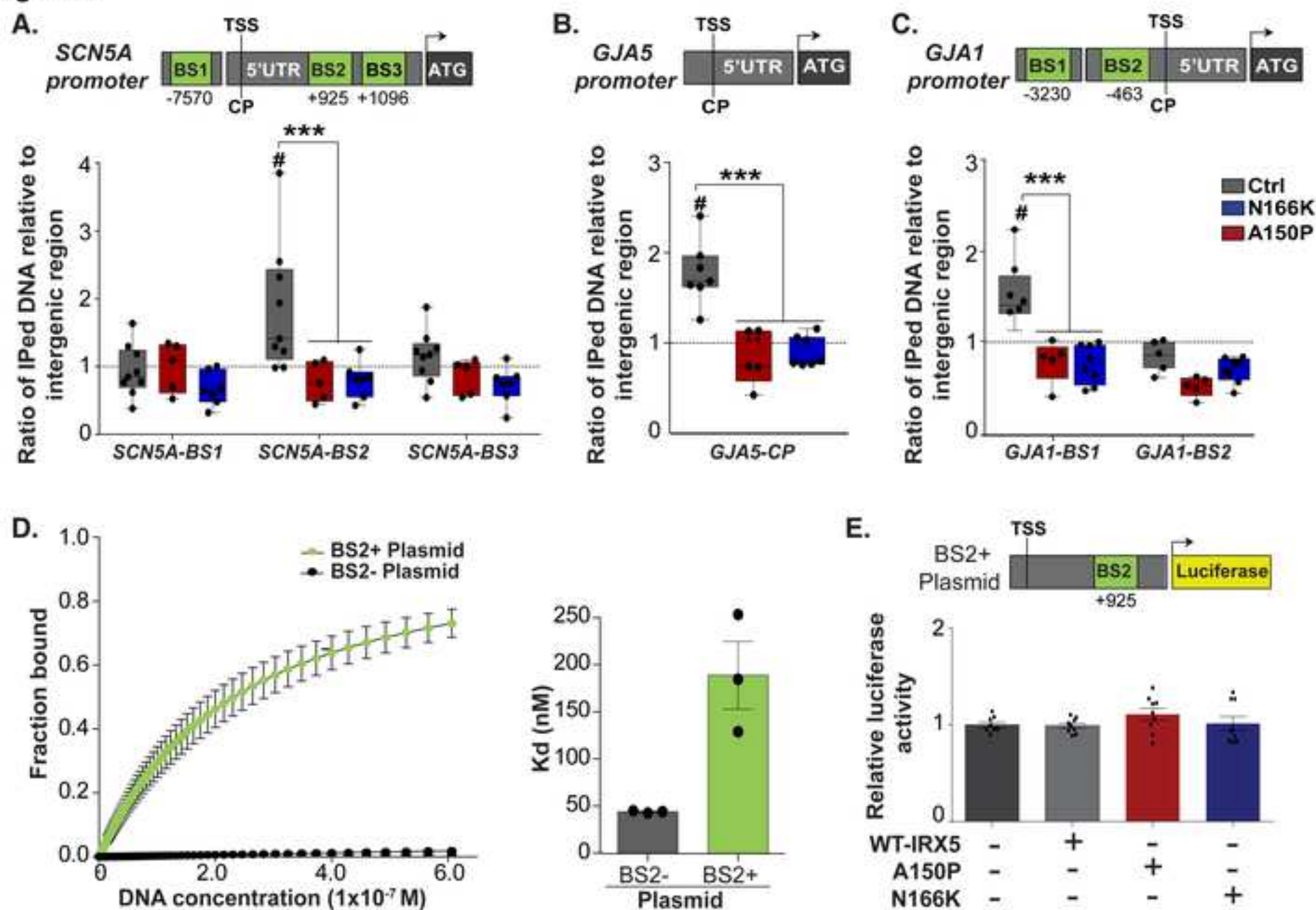
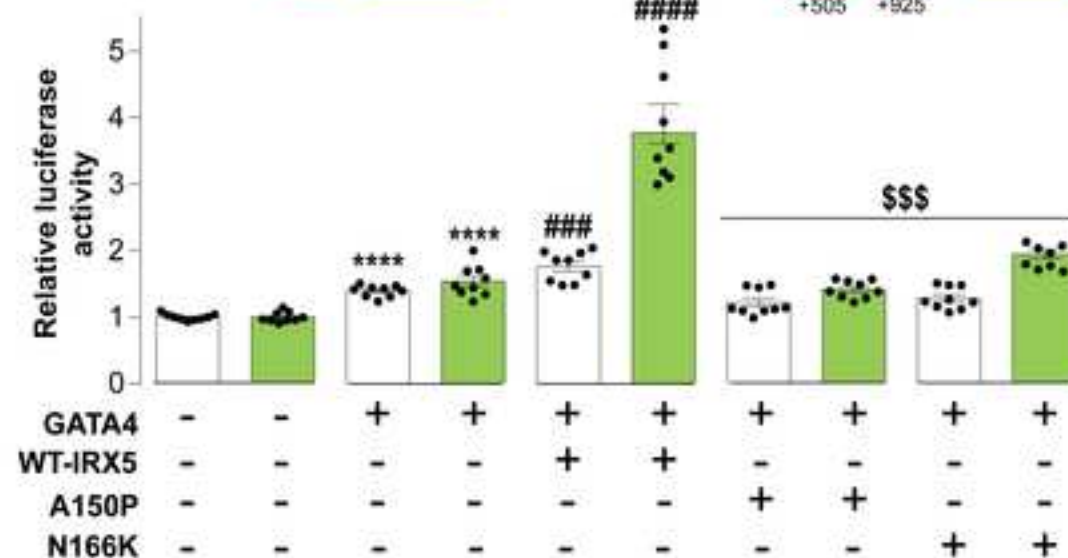
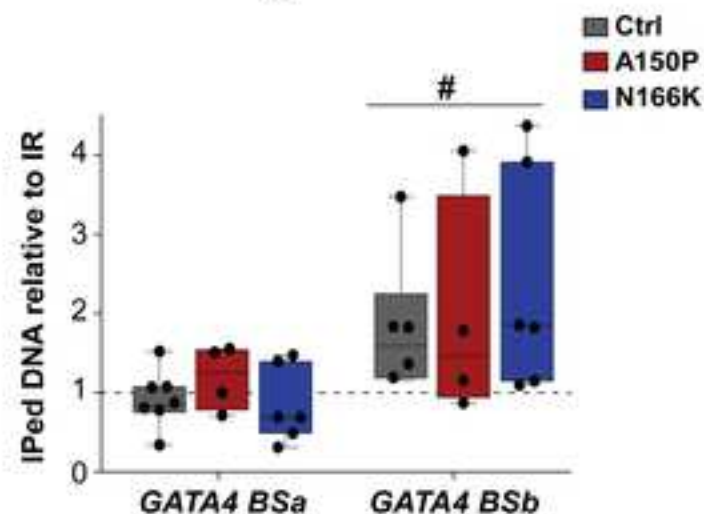
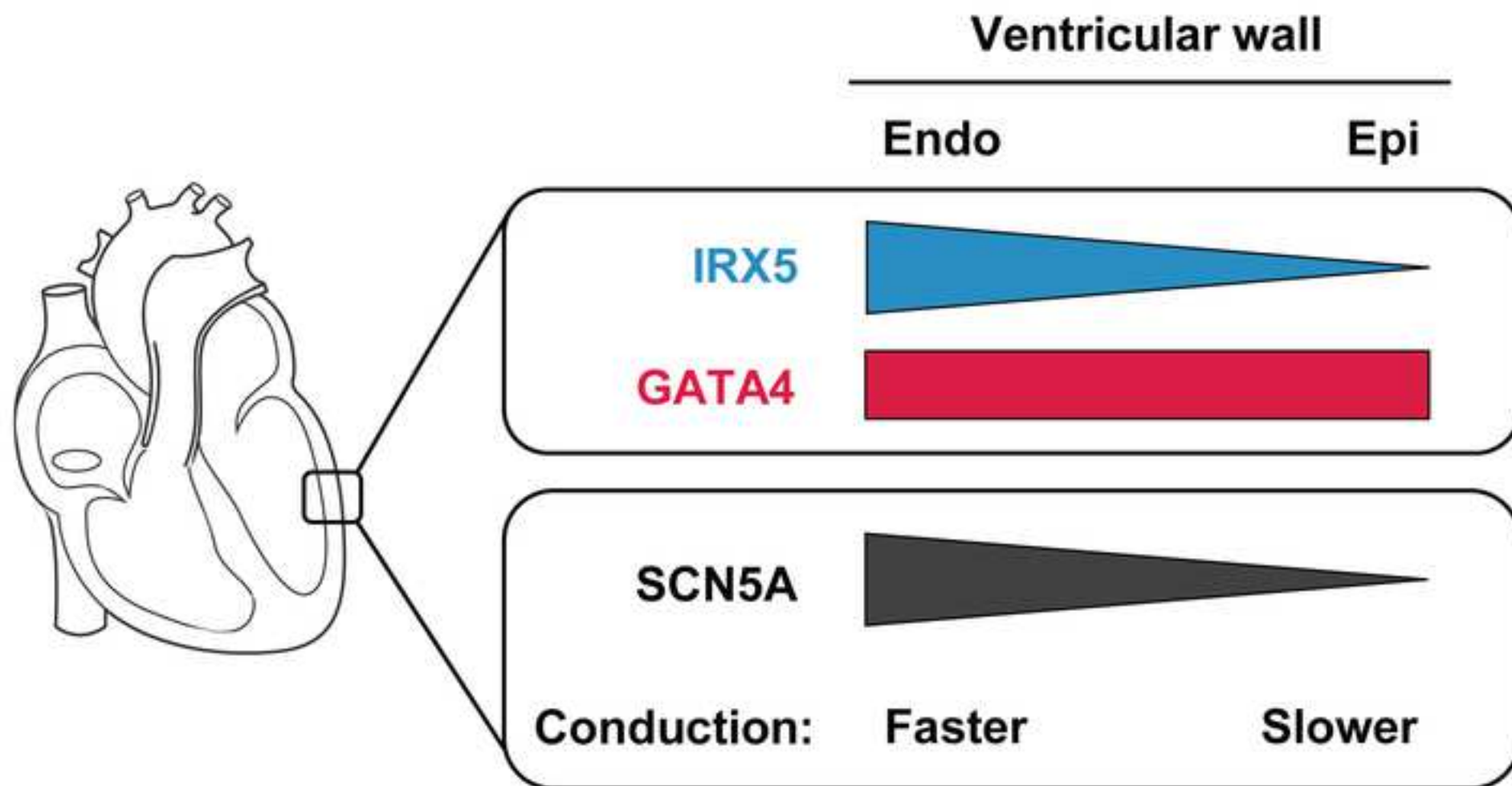
Figure 5

Figure 6



A.





Human disease model of *IRX5* mutations reveals key role for this transcription factor in cardiac conduction

Zeina R Al Sayed et al.

SUPPLEMENTAL MATERIAL

Quantitative RT-PCR

Reverse transcription of 1 µg total RNA into cDNA was achieved using the high-capacity cDNA reverse transcription Kit (Thermo Fisher Scientific). Quantitative Polymerase Chain Reactions (qPCR) were executed in duplicates using TaqMan® PCR Universal Master Mix (Thermo Fisher Scientific). TaqMan probes targeting *IRX5* (Hs04334749_m1), *SCN5A* (Hs00165693_m1), *GJA5* (Hs00270952_s1), *GJA1* (Hs00748445_s1) and *MYH7* (Hs01110632_m1) were used. Threshold cycles (Cts) were normalized to *ACTB* (Hs99999903_m1).

Immunoblotting: 2 µl NuPAGE Sample Reducing Agent and 5 µl NuPAGE LDS Sample Buffer were added to 40 µg proteins. The protein running was performed in 4-15% precast polyacrylamide gels (Bio-Rad) and proteins were then transferred onto Trans-Blot® Turbo™ Nitrocellulose Transfer Packs (Bio-Rad). Membranes were blocked using 5% non-fat milk. Expression of Cx40, Cx43, GATA4, IRX5, and Nav1.5 was revealed using respectively anti-Cx40 (Santa Cruz), anti-Cx43 (Sigma-Aldrich), anti-GATA4 (Santa Cruz), anti-Irx5 (Sigma-Aldrich) and anti-Nav1.5 (Cell signaling), and adequate secondary antibodies (Santa Cruz). Blots were revealed using chemiluminescence camera (Bio-Rad). Proteins were quantified using Image Lab software and normalized using Stain free technology or using endogenous transferrin expression.

Chromatin immunoprecipitation (ChIP): At day 28 of differentiation, beating cardiomyocyte clusters were isolated and crosslinked using 11% formaldehyde during 10 min at RT. Fixation was then stopped using 2.5M glycine for 3 min on ice. After 3 washes with PBS, cell lysis was performed using lysis buffer (10% glycerol, 140 mM NaCl, 0.5% NP40, 0.25% Triton X-100, and 1 mM EDTA) at 4°C for 10 min on a rotating platform. The cell pellets were washed with a solution containing: 200 mM NaCl, 10 mM Tris Base HCl, 0.5 mM EGTA and 1 mM EDTA. Then, the pellets were resuspended in a low salt buffer (1% Triton X-100, 140 mM NaCl, 0.1% Na deoxycholate, 0.1% SDS and 1 mM EDTA) supplemented with protease inhibitors (Sigma-Aldrich). Chromatin was sonicated with Misonix S-4000

(Qsonica). After 10 min centrifugation at 14000 rpm, supernatants were collected and incubated overnight at 4°C with 4 µg of anti-IRX5 antibody. Protein G-coated dynabeads, pre-blocked with BSA, were then added and allowed to couple with antibody-protein-DNA complexes overnight at 4°C. The dynabeads were collected, washed and then resuspended in an elution buffer (1% SDS, 50 mM Tris HCl and 10 mM EDTA). The chromatin was eluted at 65°C and then reverse-crosslinked at 65°C overnight. The DNA was treated with RNase A (Thermo Fisher) and proteinase K, purified using phenol-chloroform-isoamyl alcohol (25:24:1) and precipitated with 100% ethanol, 5 M NaCl, and 0.15 µg/µl Glycogen. SYBER green qRT-PCR method was finally performed using the designed primers (Online Table 3) to test for enrichment of the targeted sequences. Results are shown as percentage of input.

Plasmid constructs

SCN5A promoter-luciferase construct, covering the region from -261 to +613 bp of the TSS (BS2- Plasmid), contains *GATA4* *BSb* and is a kind gift from Dr. Dan Roden (Vanderbilt University, Nashville, TN, USA). A total of 459 bp were added to this construct to cover +1072 bp from TSS (BS2+ Plasmid) using the NEBuilder HiFi DNA assembly cloning kit (New England Biolabs) and following manufacturer's instructions. pCMV6-GATA4 Myc-tagged (RC210945; OriGene) and pCMV6-IRX5 GFP-tagged (RG234228; OriGene) vectors encode human GATA4 and IRX5, respectively. The A150P and N166K mutations were added to the IRX5 expressing vector using the Q5® Site-Directed Mutagenesis kit (New England Biolabs). The A150P was produced by G/C transversion at +448 using the following primers: Fw: GATCATGCTcCCATCATCACCAAGATG and Rv: TTCTCGCCCTTGGTG GGG. The N166K mutation was produced by C/A transversion at +498 using the following primers: Fw GGTTCGCCAAaGCGCGCCGGC and Rv: AGGTGGACACCTGGGTGAGGG.

Supplemental Figures:

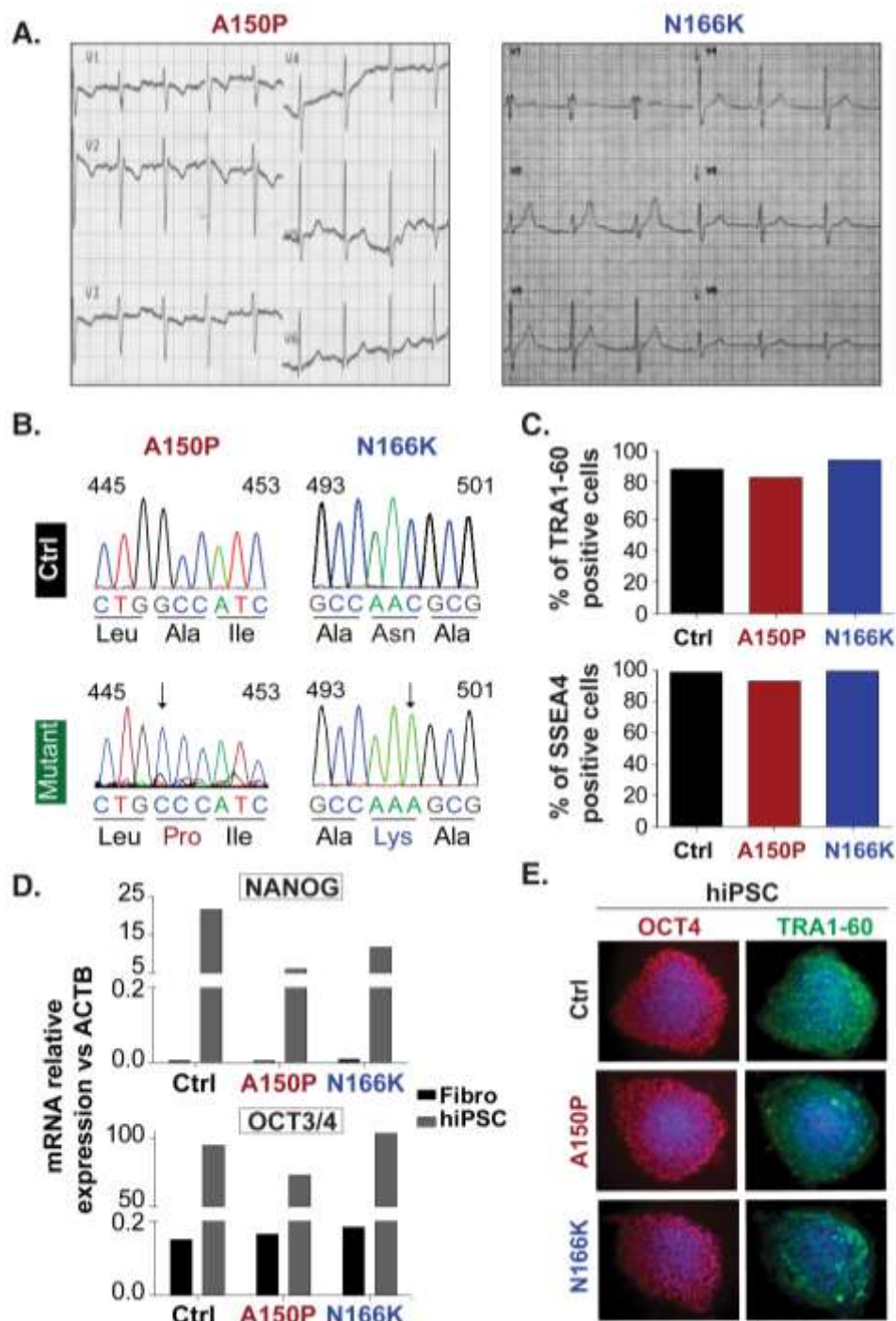


Figure S1: Validation of hiPSCs derived from Hamamy syndrome-affected patients.

- A. Leads V1 to V6 from electrocardiogram (ECG) of patients carrying A150P- and N166K-*IRX5* mutations. Conduction defect presented by Right Bundle Branch Block at the V1 lead and QRS prolongation is visible in both patient ECG.
- B. Genomic sequence chromatograms validate the presence of c.448G>C and c.498C>A *IRX5* mutations in mutant hiPSCs but not in control hiPSCs.

- C. Flow cytometry quantification of pluripotent stem cell markers TRA1-60 and SSEA4 in control and *IRX5*-mutated hiPSCs.
- D. mRNA expression levels of endogenous pluripotent stem cell markers, NANOG and OCT3/4, in control and *IRX5*-mutated hiPSCs as compared to their corresponding skin fibroblasts (Fibro) using TaqMan® technique.
- E. Representative immunostainings of endogenous OCT4 nuclear pluripotency marker and TRA1-60 pluripotency marker expressed at the membrane. Nuclei are stained in blue by DAPI.

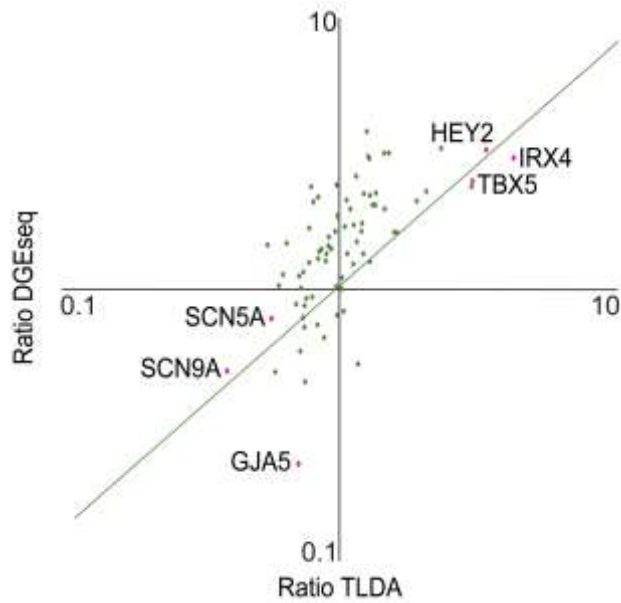


Figure S2: TLDA and 3'SRP data are correlated.

Ratios of mRNA expression in *IRX5*-mutated over control hiPS-CMs for 93 genes selected for TLDA analysis. For each gene, ratio obtained by TLDA was plotted in X coordinate and ratio obtained by 3'SRP was plotted in Y coordinate. Green Line represents identity line. Examples of genes relevant to cardiac conduction are shown in pink. For instance, *IRX4* increased according to both 3'SRP and TLDA (3X vs 4.2X, respectively) whereas *SCN5A*, *SCN9A* and *GJA5* decreased according to both 3'SRP and TLDA (1.3X vs 1.8X; 2X vs 2.5X and 4.3X vs 1.4X, respectively).

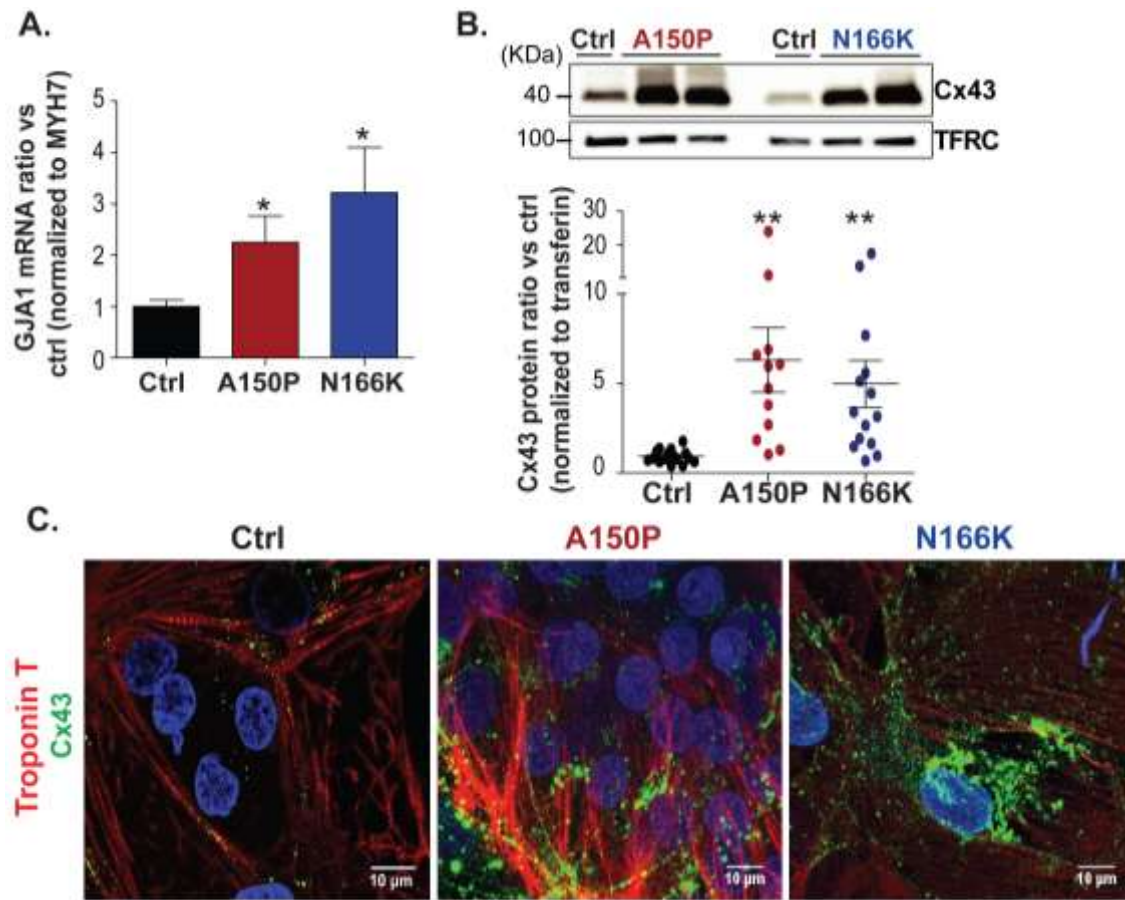


Figure S3: Cx43 ectopic expression in both A150P- and N166K-hiPS-CMs.

- A. TaqMan quantification of GJA1 transcript expression. Cts were normalized to MYH7, a myosin specific to ventricular cardiomyocytes. Ctrl n=19; A150P n=8; N166K n=8. * $p < 0.05$ vs. control (t test).
- B. Representative immunoblot showing Cx43 protein expression with corresponding transferrin (transf) expression in A150P and N166K *IRX5*-mutated and control hiPS-CMs. Ratio of Cx43 expression level (normalized to transferrin expression level) in A150P (n=12) and N166K (n=14) *IRX5*-mutated hiPS-CMs vs. control hiPS-CMs (n=16). ** $p < 0.01$ vs. control (t test).
- C. Immunostainings illustrating Cx43 expression and localization (green) in Troponin T (red) positive hiPS-CMs, merged with a nuclear staining using DAPI (blue)

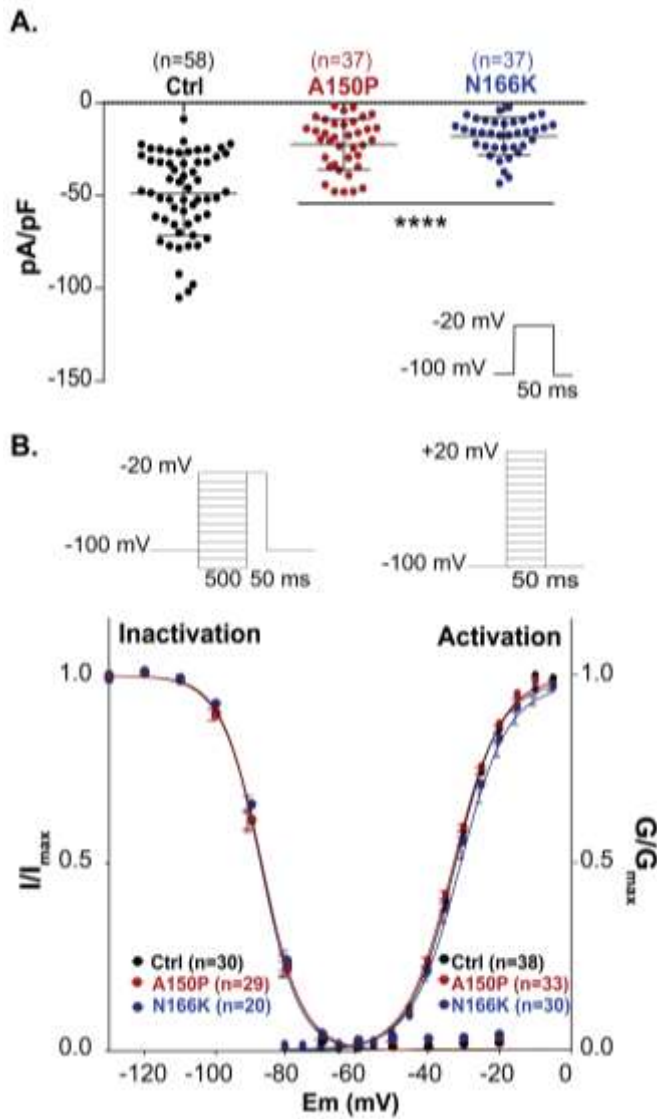


Figure S4: I_{Na} density was reduced in *IRX5*-mutated hiPS-CMs with no change in activation and inactivation parameters.

A. Current densities measured in control and *IRX5*-mutated hiPS-CMs, determined at -20 mV.

**** $p < 0.0001$ vs. control (t test).

B. I_{Na} voltage dependence of activation and steady-state inactivation (respective protocols depicted in insets).

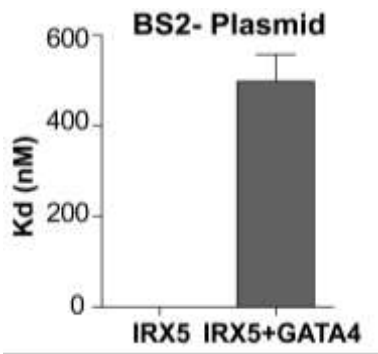


Figure S5: In contrast with IRX5 alone, the complex GATA4-IRX5 was able to bind to *SCN5A* plasmid lacking BS2

MST analysis of dissociation constant for interaction between *SCN5A* promoter (BS2- Plasmid) and IRX5 alone or IRX5 + GATA4. Protein lysates were prepared from HEK293T transfected with either IRX5-GFP only or both IRX5-GFP and GATA4 expressing vectors. Binding was tested with different concentrations of BS2- Plasmid containing *GATA4 BSb* but not *IRX5 BS2* (n=2 per group).

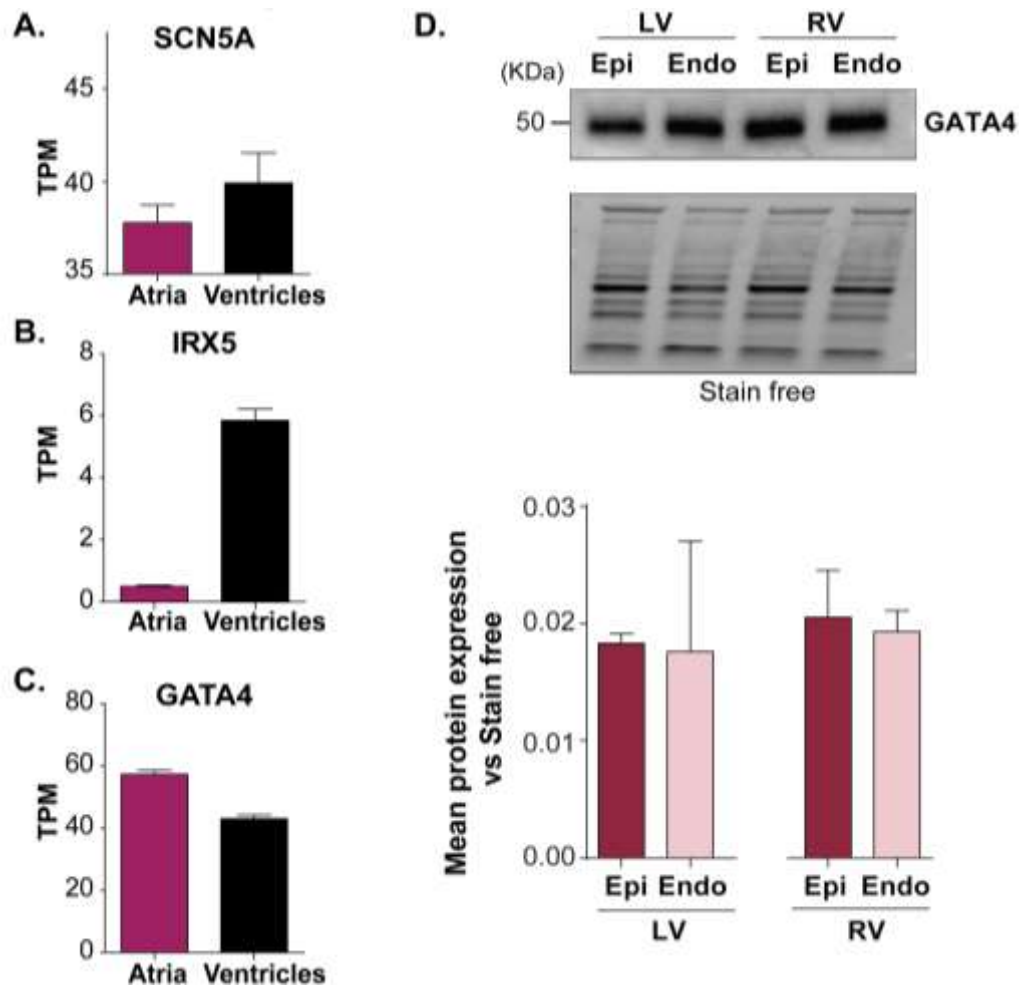


Figure S6: IRX5 but not GATA4 has a comparable expression profile to SCN5A.

A, B and C represents respectively transcriptomic profiles of SCN5A, IRX5 and GATA4 in atrial and ventricular human tissues, respectively. TPMs were obtained from GTEx database (n=297 and 303 for atrial and ventricular tissues, respectively).

D. Top: Representative immunoblot of GATA4 expression levels in protein lysates of ventricular sub-endocardial (Endo) and sub-epicardial (Epi) samples obtained from three human left (LV) and right ventricles (RV). Bottom: GATA4 protein expression level quantifications (n=3 per group), normalized to Stain free.

Supplemental Tables

Supplemental Table 1. Primer sequences used to validate mutations in mutant hiPSCs.

	Sequence
IRX5A150P-F	ccctgggatcgtacccttac
IRX5A150P-R	ggcgtccacgtcattttatt
IRX5N166K-F	aacgagcaccgcaagaac
IRX5N166K-R	gtcctcgtcgttcttctcca

Supplemental Table 1. A. Murine tissue TLDA probe references and corresponding genes. B. Human iPS-CMs TLDA probe references and corresponding genes.

A		B	
Transcription factors		Ion channels	
18S	Mm03928990_g1	18S	Mm03928990_g1
Arnt	Mm00507836_m1	Abcc9	Mm00441638_m1
Arntl	Mm00500226_m1	Actc1	Mm00477277_g1
Atfb1	Mm00464368_m1	Ank2	Mm00618325_m1
Atf1	Mm00657594_m1	Atpia1	Mm00523255_m1
Atf2	Mm00833804_g1	Atp1b1	Mm00437612_m1
Atf3	Mm00476032_m1	Atp2a2	Mm00437634_m1
Atf4	Mm00515324_m1	Bop	Mm00477663_m1
Bach1	Mm00476077_m1	Cacna1c	Mm00437917_m1
Bcl11a	Mm00479358_m1	Cacna1d	Mm00551384_m1
Bcl6	Mm00477633_m1	Cacna1g	Mm00486549_m1
Bcl6b	Mm00455914_m1	Cacna1h	Mm00445369_m1
Cacna1c	Mm00437917_m1	Cacna2d1	Mm00486607_m1
Cacna1d	Mm00551384_m1	Cacna2d2	Mm00457825_m1
Cacna1g	Mm00486549_m1	Cacna2d3	Mm00486613_m1
Cacna2d1	Mm00486607_m1	Cacnb1	Mm00518940_m1
Cacna2d2	Mm00457825_m1	Cacnb2	Mm00659092_m1
Cacnb3	Mm00432233_m1	Cacnb3	Mm00432233_m1
Cbfa2t1h	Mm00486771_m1	Cacng7	Mm00519216_m1
Cited1	Mm00455934_m1	Calml1	Mm00486655_m1
Cited2	Mm00516121_m1	Calms3	Mm00482929_m1
Cnbp1	Mm00488938_m1	Casq2	Mm00486738_m1
Cops2	Mm00487179_m1	Cd4	Mm00442754_m1
Cops5	Mm00489065_m1	Cfr	Mm00445197_m1
Creb1	Mm00501607_m1	Clcn2	Mm00438245_m1
Creb3	Mm00457268_m1	Clcn3	Mm00432566_m1
Crem	Mm00516346_m1	Cnn1	Mm0047032_m1
Cri1	Mm00517974_s1	Col6a1	Mm00487160_m1
Cutl1	Mm00501628_m1	Dlgh1	Mm00492174_m1
Dazap2	Mm00726901_s1	Dlgh4	Mm00492193_m1
Ddx20	Mm00600300_g1	Elf4g2	Mm00469036_m1
Dmr12	Mm00659912_m1	G6pdx	Mm00656735_g1
E2f1	Mm00432939_m1	Gapd	Mm005999915_g1
E2f2	Mm00624964_m1	Gata4	Mm00484689_m1
E2f4	Mm00514160_m1	Gja1	Mm00439105_m1
E2f5	Mm00468171_m1	Gja4	Mm00433610_s1
E2f6	Mm00519030_m1	Gja5	Mm00433619_s1
E4f1	Mm00468177_m1	Gja7	Mm00433624_m1
Elf4g2	Mm00469036_m1	Hcn1	Mm00468832_m1
En2	Mm00438710_m1	Hcn2	Mm00468538_m1
Ep300	Mm00625535_m1	Hcn3	Mm00468543_m1
Erg	Mm00504897_m1	Hprt	Mm00446968_m1
Esr1	Mm00433149_m1	Hsp86	Mm00658568_gH
Esr2	Mm00516267_m1	Hspa1	Mm00442854_m1
Ets2	Mm00468972_m1	Il6	Mm00446190_m1
Etv1	Mm00514804_m1	Itpr2	Mm00444937_m1
Fkhl18	Mm00809617_s1	Kcna1	Mm00439977_s1
Flil1	Mm00484410_m1	Kcna2	Mm00434584_s1
Fos	Mm00487425_m1	Kcna4	Mm00445241_s1
Foxa3	Mm00484714_m1	Kcna5	Mm00524346_s1
Foxc2	Mm00546194_s1	Kcna6	Mm00496625_s1
Foxk1	Mm00440301_m1	Kcnab1	Mm00440018_m1
Foxm1	Mm00514924_m1	Kcnab2	Mm00440022_m1
Foxo1	Mm00490672_m1	Kcnb1	Mm00492791_m1
Fus	Mm00836363_g1	Kcnd1	Mm00492796_m1
Gabpa	Mm00484598_m1	Kcnd2	Mm00498065_m1
Gapdh	Mm005999915_g1	Kcnd3	Mm00498260_m1
Gata1	Mm00484678_m1	Kcne1	Mm00434615_m1
Gata3	Mm00484683_m1	Kcne1l	Mm00517596_s1
Gata4	Mm00484689_m1	Kcne2	Mm00506492_m1
Gata5	Mm00484692_m1	Kcne3	Mm00445119_m1
Gata6	Mm00802636_m1	Kcnh2	Mm00465370_m1
Gja1	Mm00439105_m1	Kcnip1	Mm00471928_m1
Gja5	Mm00433619_s1	Kcnip2	Mm00518914_m1
Gja7	Mm00433624_m1	Kcnj11	Mm00440050_s1
Gtf2i2r1	Mm00465654_m1	Kcnj12	Mm00440058_s1
Hand1	Mm00433931_m1	Kcnj2	Mm00434616_m1
Hand2	Mm00439247_m1	Kcnj3	Mm00434618_m1
Hcn2	Mm00468538_m1	Kcnj8	Mm00434620_m1
Hes1	Mm00468601_m1	Kcnk2	Mm00440072_m1
Hey1	Mm00468865_m1	Kcnn1	Mm00446259_m1
Hey2	Mm00469280_m1	Kcnn2	Mm00446514_m1
Heyl	Mm00516555_m1	Kcnp1	Mm00434641_m1
Hif1a	Mm00468869_m1	Myh7	Mm00600555_m1
Hlx	Mm00468656_m1	Myia	Mm00440378_m1
Hoxa13	Mm00433967_m1	Mylic2a	Mm00491655_m1
Hoxa9	Mm00439364_m1	Myipc	Mm00440384_m1
Hprt	Mm00446968_m1	Nkx2-5	Mm00657783_m1
Hsf1	Mm00801771_g1	Nppb	Mm00435304_g1
Htatip	Mm00724374_m1	Pias3	Mm00450739_m1
Irx3	Mm00500463_m1	Pln	Mm00452263_m1
Irx4	Mm00502170_m1	Pou5f1	Mm00658129_gH
Irx5	Mm00502107_m1	Prkaca	Mm00660092_m1
Isgf3g	Mm00492679_m1	Prkce	Mm00440894_m1
Jun	Mm00495062_s1	Ryr2	Mm00465877_m1
Jund1	Mm00495088_s1	Scn1b	Mm00441210_m1
Jund2	Mm00473044_m1	Scn3a	Mm00658167_m1
Klf13	Mm00727486_s1	Scn3b	Mm00463369_m1
Klf15	Mm00517792_m1	Scn4a	Mm00500103_m1
Klf16	Mm00625334_m1	Scn5a	Mm00451971_m1
Klf2	Mm00500486_g1	Slc8a1	Mm00441524_m1
Mafk	Mm00456782_m1	Tgfb1	Mm00441724_m1
Polr2a	Mm00839493_m1	Tnni3	Mm00437164_m1
Scn1b	Mm00441210_m1	Tnni2	Mm00441922_m1
Scn3b	Mm00463369_m1	Uchl1	Mm00495900_m1
Scn5a	Mm00451971_m1	Ywhae	Mm00494246_m1

Human TLDA	
ABCC8	Hs01093761_m1
ABCC9	Hs00245832_m1
ATP1A3	Hs00958036_m1
ATP1B1	Hs00426868_g1
ATP2A2	Hs00544877_m1
ATP2A3	Hs00193090_m1
ATP2B4	Hs00608066_m1
CACNA1C	Hs0167681_m1
CACNA1D	Hs0167753_m1
CACNA1G	Hs0367969_m1
18S	Hs99999901_s1
CACNA1H	Hs01103527_m1
CACNA2D1	Hs00984856_m1
CACNA2D2	Hs01021049_m1
CACNB2	Hs01100744_m1
CALM1	Hs00300085_s1
CALM3	Hs00968732_g1
CASQ2	Hs00154286_m1
GJA1	Hs00748445_s1
GJA5	Hs00270952_s1
GJC1	Hs00271416_s1
GJD3	Hs00987388_s1
HCN1	Hs01085412_m1
HCN2	Hs00606903_m1
HCN3	Hs0380018_m1
HCN4	Hs00975492_m1
ITPR1	Hs0181881_m1
ITPR3	Hs00609908_m1
KCNA2	Hs00270656_s1
KCNA4	Hs00937357_s1
KCNA5	Hs00969279_s1
KCNA7	Hs00361015_m1
KCNAB2	Hs00186308_m1
KCNAB3	Hs01085073_m1
KCNB1	Hs00270657_m1
KCN4	Hs00428198_m1
KCND2	Hs01054873_m1
KCND3	Hs00542597_m1
KCNE1	Hs00264799_s1
KCNE1L	Hs01085745_s1
KCNE2	Hs00270822_s1
KCNE3	Hs01921543_s1
KCNE4	Hs01851577_s1
KCNH2	Hs04234270_g1
KCNIP2	Hs01552688_g1
KCNJ11	Hs00265026_m1
KCNJ2	Hs01876357_s1
KCNJ3	Hs04334861_m1
KCNJ4	Hs00705379_s1
KCNJ5	Hs00168476_m1
KCNJ8	Hs00958961_m1
KCNK1	Hs00158428_m1
KCNK3	Hs00605529_m1
KCNK5	Hs00186652_m1
KCNQ1	Hs00923522_m1
NPPA	Hs00383230_g1
NPPB	Hs01057466_g1
PLN	Hs01848144_s1
PPP3CA	Hs00174223_m1
RYR2	Hs00181461_m1
SCN10A	Hs01045137_m1
SCN1B	Hs03987893_m1
SCN2B	Hs00394952_m1
SCN3A	Hs00366913_m1
SCN3B	Hs01024483_m1
SCN4A	Hs01109480_m1
SCN4B	Hs03681025_m1
SCN5A	Hs00165693_m1
SCN7A	Hs00161546_m1
SCN9A	Hs00161567_m1
SLC8A1	Hs01062258_m1
ANK2	Hs00153998_m1
ACTB	Hs99999903_m1
RPL13A	Hs04194366_g1
GATA3	Hs00231122_m1
GATA4	Hs00171403_m1
GATA5	Hs00388359_m1
GATA6	Hs00232018_m1
HEY2	Hs00232622_m1
IRX3	Hs01124217_g1
IRX4	Hs00212560_m1
IRX5	Hs04334749_m1
TBX2	Hs00911929_m1
TBX3	Hs00195612_m1
TBX5	Hs00361155_m1
NKX2-5	Hs00231763_m1
TNNI3	Hs00165957_m1
TNNI2	Hs00943911_m1
MYH6	Hs01101425_m1
MYH7	Hs01110632_m1
RRAD	Hs00188163_m1
CLASP2	Hs00380556_m1
GPD1L	Hs00380518_m1
B2M	Hs00187842_m1
MYL7	Hs01085598_g1
MYL2	Hs00166405_m1

Supplemental Table 3. Primers used to amplify DNA after ChIP for IRX5.

	Primer sequences	Position relative to TSS
IRX5- <i>SCN5A</i> -BS1	Fw: tacctgcacaccattctccc Rv: agagggtcagggtgagagat	-7611 -7527
IRX5- <i>SCN5A</i> -BS2	Fw: ttctctgccctcctctctct Rv: cgccaccaaagacgatcaaa	+847 +929
IRX5- <i>SCN5A</i> -BS3	Fw: ttgatcgtctttggtggcg Rv: atctgatctggctgtgctc	+929 +1112
IRX5- <i>GJA5</i> -CP	Fw: agccctccttcattcactc Rv: ctgtctgtgttctccagga	-55 +48
IRX5- <i>GJA1</i> -BS1	Fw: ctcttcagcaggtcagtc Rv: gacaaggaagaggaggctgt	-3272 -3186
IRX5- <i>GJA1</i> -BS2	Fw: tctctctcccatccacca Rv: agaggtaggtgtgagtgacc	-490 -412
GATA4- <i>SCN5A</i> -BSa	Fw: ccgcctatgtctgtctgtcc Rv: gcacactcccacactgacc	-268 -201
GATA4- <i>SCN5A</i> -BSb	Fw: cccttccttccttctt Rv: ggtatccgggtcccaatcc	+416 +529
Intergenic region	Fw: agcaccatgataagaaagcca Rv: acccaacagaaatgaaagcct	

TSS: Transcription Start Site; Fw: Forward; Rv: Reverse.

Supplemental Table 4. Solutions used for patch clamp recordings (mM).

	Solution AP		Solution I _{Na}		Solution I _{Ca,L}		AP clamp I _{Na}	
	Intra-pipette	Extra-cellular	Intra-pipette	Extra-cellular	Intra-pipette	Extra-cellular	Intra-pipette	Extra-cellular
Kgluconate	125							
NaCl	5	140	3	20	5		3	130
KCl	20	4						
Hepes	5	10	5	10	10	10	5	10
Glucose		10						
MgCl ₂		0.5	2	1.2		1	2	1
CaCl ₂		1			2	5		
CsCl			133	110	145		133	10
EGTA			10		5		10	
TEACL			2			160	2	
Na ₂ ATP			2				2	
CoCl ₂				1.8				1.8
Mannitol				30		20		30
MgATP					5			
TTX						0.03		

Supplemental Table 5. Sodium current V50, voltage of halfmaximum activation and inactivation, and K, slope factor. Data are presented as mean \pm SD.

			Ctrl	A150P	N166K
I_{Na}	Activation	V50	-31.51 (\pm 0.21)	-32.19 (\pm 0.32)	-31.09 (\pm 0.34)
		K	6.452 (\pm 0.17)	6.526 (\pm 0.25)	6.736 (\pm 0.26)
	Inactivation	V50	-87.27 (\pm 0.21)	-87.37 (\pm 0.23)	-86.36 (\pm 0.25)
		K	-5.674 (\pm 0.18)	-5.774 (\pm 0.20)	-5.508 (\pm 0.21)